Kaunas University of Technology

Faculty of Mathematics and Natural Sciences

Development of Iodine Enriched Occasional Radiation Exposure Indicators

Master's Final Degree Project

Gabrielius Stankus

Project author

Prof. dr. Diana Adlienė

Supervisor

Kaunas, 2025

Kaunas University of Technology

Faculty of Mathematics and Natural Sciences

Development of Iodine Enriched Occasional Radiation Exposure Indicators

Master's Final Degree Project

Medical Physics (6213GX001)

Gabrielius Stankus

Project author

Prof. dr. Diana Adlienė

Supervisor

Assoc. prof. dr. Jurgita Čyvienė

Reviewer

Kaunas, 2025

Kaunas University of Technology

Faculty of Mathematics and Natural Sciences
Gabrielius Stankus

Development of Iodine Enriched Occasional Radiation Exposure Indicators

Declaration of Academic Integrity

I confirm the following:

1. I have prepared the final degree project independently and honestly without any violations of the copyrights or other rights of others, following the provisions of the Law on Copyrights and Related Rights of the Republic of Lithuania, the Regulations on the Management and Transfer of Intellectual Property of Kaunas University of Technology (hereinafter – University) and the ethical requirements stipulated by the Code of Academic Ethics of the University;

2. All the data and research results provided in the final degree project are correct and obtained legally; none of the parts of this project are plagiarised from any printed or electronic sources; all the quotations and references provided in the text of the final degree project are indicated in the list of references;

3. I have not paid anyone any monetary funds for the final degree project or the parts thereof unless required by the law;

4. I understand that in the case of any discovery of the fact of dishonesty or violation of any rights of others, the academic penalties will be imposed on me under the procedure applied at the University; I will be expelled from the University and my final degree project can be submitted to the Office of the Ombudsperson for Academic Ethics and Procedures in the examination of a possible violation of academic ethics.

Gabrielius Stankus

Confirmed electronically

Stankus Gabrielius. Development of iodine enriched occasional radiation exposure indicators. Master's Final Degree Project / supervisor prof. dr. Diana Adlienė; Faculty of Mathematics and Natural Sciences, Kaunas University of Technology.

Study field and area (study field group): Medical Technologies (Health Sciences).

Keywords: radiation indicators; hydrogels; colored polymer films.

Kaunas, 2025. 51 pages.

Summary

Accidental exposure to ionizing radiation, in particular γ-rays, can result from various sources: equipment malfunction, leakage from radiation sources or even hostile action, involving radioactive materials. While occupational exposure is well-regulated, the detection and assessment of unintentional exposure remains a challenge due to the limitations of existing monitoring technologies, which are often costly, complex or lack sensitivity.

In this work poly(vinyl alcohol)-iodide (PVA-I) gel colored indicators, sensitive within the 0.2 – 10 Gy range, are proposed as a simple, cost-effective, and portable solution to address the need of immediate monitoring devices that could be distributed to the broad public in the case of nuclear accidents or radiological pollution, which otherwise may cause irreversible harm to any living organism.

Two types of film and three types of solution indicators were fabricated. The sensitivity of F2 (0.45 w% KIO_3) films, according to the ~340 nm absorbance maximum of triiodide ions, was only 0.0429 Gy^{-1}. According to the ~490 nm absorbance maximum of PVA-triiodide complex, S2 (2 w% KI) indicator samples had a sensitivity of 0.0058 Gy^{-1} and S3 (5 w% KI) indicator samples had a sensitivity of 0.0135 Gy^{-1}, which was comparable to a similar composition indicator sensitivity (0.010 Gy^{-1}), described in literature. However, additional experiments must be done to ensure a better sensitivity to radiation and more resistance to ambient conditions, such as light, air and temperature.

Stankus Gabrielius. Jodu praturtintų spindulinės atsitiktinės apšvitos indikatorių kūrimas. Magistro baigiamasis projektas / vadovė prof. dr. Diana Adlienė; Kauno technologijos universitetas, matematikos ir gamtos mokslų fakultetas.

Studijų kryptis ir sritis (studijų krypčių grupė): Medicinos technologijos (Sveikatos mokslai).

Reikšminiai žodžiai: radiacijos indikatoriai; hidrogeliai; spalvotos polimerinės plėvelės.

Kaunas, 2025. 51 p.

Santrauka

Atsitiktinis jonizuojančiosios spinduliuotės, ypač gama spindulių, poveikis gali kilti dėl įvairių priežasčių: įrangos gedimo, nuotekinės spinduliuotės iš radiacijos šaltinių ar net priešiškų veiksmų, susijusių su radioaktyviosiomis medžiagomis. Nors profesinė apšvita yra griežtai reguliuojama, atsitiktinės apšvitos aptikimas ir įvertinimas dar vis yra sudėtingas procesas dėl esamų radiacijos stebėsenos technologijų trūkumų: jos dažnai reikalauja brangių komponentų, yra sudėtingai pagaminamos arba nepakankamai jautrios.

Šiame darbe siūlomi spalvoti polivinilo alkoholio-jodido (PVA-I) gelio indikatoriai, jautrūs 0.2 – 10 Gy intervale, kaip paprastas, pigus ir nešiojamas sprendimas, skirtas patenkinti skubios stebėsenos poreikius, kuris galėtų būti paplatintas visuomenei branduolinių avarijų ar radiologinės taršos atvejais kaip apsauga nuo negrįžtamos radiacijos žalos.

Buvo paruošti dviejų tipų plėvelių ir trijų tipų tirpalų indikatoriai. F2 (0.45 w% KIO_3) plėvelių jautrumas, vertinant pagal laisvų trijodido jonų ~340 nm absorbcijos maksimumą, siekė 0.0429 Gy^{-1}. Vertinant pagal PVA-trijodido komplekso ~490 nm absorbcijos maksimumą, S2 (2 w% KI) indikatoriaus jautrumas buvo 0.0058 Gy^{-1}, o S3 (5 w% KI) indikatoriaus jautrumas – 0.0135 Gy^{-1}, kuris yra panašus į analogiškos sudėties indikatorių, aprašytų literatūroje, jautrumą (0.010 Gy^{-1}). Vis dėlto būtina atlikti papildomus eksperimentus, siekiant patobulinti indikatorių jautrumą jonizuojančiajai spinduliuotei ir atsparumą aplinkos veiksniams (šviesai, orui, temperatūrai).

Table of contents

List of figures

List of tables

Introduction

Accidental irradiation, most often in the form of γ-rays, may happen as a result of leakage from various radiation sources, during quality assurance measurements of instruments such as particle accelerators, computed tomography scanners or even – nuclear warfare. Thus, the detection of incident exposure is relevant not only for radiation oncologists and medical physicists, but even in the context of worldwide conflict, creating tension because of plausible disregard of nuclear safety. Occupational exposure is regulated [1], however measurement and evaluation of accidental exposure, rising from inadvertent or premeditated radioactive pollution or equipment failure, is problematic [2]. To address this matter, a large variety of radioactivity registration methods and devices can be utilized, but many are either not sensitive enough, are quite complex or require expensive electronics [3–5]. There is a lack of simple and relatively cheap individual indicators alerting about increased radiation levels. A promising novel concept would be the application of colored detectors, that change their optical properties depending on the absorbed dose. It is important that these indicators can be affixed to the clothing of persons and alert about increased radioactivity in the surrounding environment [6] [7]. For this purpose a promising PVA-iodide indicator is proposed in this work, which changes its optical properties from a clear solution to a faint red color in the dose range of 0.2 – 10 Gy. This type of PVA-I gel offers advantages such as simplicity, portability and cost-effectiveness. However, additional experiments must be done to ensure a better sensitivity to radiation and more resistance to ambient conditions, such as light and temperature.

The aim of this work is to develop PVA based hydrogels, sensitive to occasional radiation exposure.

In order to implement this aim the following tasks should be fulfilled:

1. to develop polymer-based radiation indicators containing iodine;
2. to evaluate changes in the optical properties of fabricated radiation indicators, irradiated with X-ray photons in the 0.2 Gy – 10 Gy dose range;
3. to assess the dose sensitivity of fabricated radiation indicators, according to the variations in their optical properties after irradiation.

1. Literature review

1. 1. Incident radiation

Radiological pollution refers to an increase of natural radiation to harmful levels, caused by anthropogenic activities. This process is differentiated into three categories. Firstly, continuous radioactive contamination occurs because of mining, refining and utilizing radioactive materials. Secondly, occasional radiological pollution is related with nuclear tests of experiments. An example of this can be atmospheric nuclear tests from the mid 20th century [8]. Lastly, accidental radioactive contamination is the most dangerous due to its unpredictability and is caused by nuclear infrastructure failures, improper handling of radioactive materials or other unforeseeable catastrophic events. All of these types of pollution can result in short and long-term damage of tissues, as cells get affected at the molecular level [9]. However, radioactive contamination may cause irreparable harm, thus radiological monitoring programs are required to ensure that public exposure does not exceed allowed limits, which are usually delineated as an annual effective dose of 1 mSv [10]. Nevertheless, even though monitoring of radiation levels is in effect, it is not immediate. Thus, the value and potential of incident radiation indicators, rapidly changing their optical characteristics as a consequence of radiation exposure, cannot be underestimated.

During major nuclear accidents (for example, Chernobyl and Fukushima accidents) the most important radionuclides, that can pose harm to living individuals and the environment, are iodine-131, cesium-134, cesium-137, ant strontium-90. Radiation properties of these radionuclides are described in Table 1. Other radionuclides are also released, but they are either short-lived, short-ranged, or emitted in too small amounts [11]. To understand the harm of radionuclides the effective half-life measure is used to assess the time, during which half of radionuclides' amount is eliminated from the body via physical decay and biological excretion. Strontium-90 has quite a long effective half-life, and it accumulates mostly in the bones by interchanging with calcium in hydroxyapatite ($Ca_{10}(PO_4)_6(OH)_2$) structure as a result of chemical similarities between these two elements [12]. Cesium-134 and 137 are also chemically similar to potassium; that is why the uptake of these radioisotopes is quite high in humans and in plants [13], even reaching bioavailability of 80 % in animals [14]. Although iodine has a short effective half-life, 10 – 30 % of it accumulates in the thyroid, exposing it to beta particles [11].

Table 1. Most common radionuclides, posing health concerns, released during nuclear accidents [11]

	Sr-90	**I-131**	**Cs-134**	**Cs-137**
Decay type	β	β, γ	β, γ	β, γ
Maximal energy of emitted particles (abundance) [15]	546 keV (100 %)	β – 606 keV (89 %); γ – 364 keV (81 %)	β – 658 keV (70 %); γ – 605 keV (98 %)	β – 512 keV (94 %); γ – 662 keV (85 %)
Biological half-life	50 years	80 days	70 – 100 days	70 – 100 days
Physical half-life	28.8 years	8 days	2.1 years	30 years
Effective half-life	18 years	7 days	64 – 88 days	70 – 99 days
Accumulating tissues	Bones	Thyroid	Whole body	Whole body

Interestingly, the most dominant radionuclide that is released during nuclear accidents is ^{133}Xe , with $11 \cdot 10^{18}$ Bq, $6.5 \cdot 10^{18}$ Bq and $12 \cdot 10^{18}$ Bq being released during Fukushima, Chernobyl and Windscale Fire accidents correspondingly [11] [16]. However, ^{133}Xe is less dangerous than bioaccumulated radionuclides, as the biological half-life of ^{133}Xe is only 30 seconds, because less than 15 % of inhaled radioxenon is absorbed and the energies emitted are quite small (101 keV for beta decay (99 %) and 81 keV for gamma decay (37 %)). The physical half-life of ^{133}Xe is not that long as well (~5 days). Chemically ^{133}Xe is a noble gas, which is physiologically inert, since it has a full valence shell [17]. Tritium has a longer half-life (12.3 years) than xenon, but its relevancy is similar to radioxenon's in the sense that it releases low energy beta particles (18.6 keV (100 %)), that can travel only about 6 mm in air [11].

Another reason why the radionuclides in Table 1 are so dangerous is their ease of propagation and persistence in the environment. For instance, as a consequence of cesium's relatively low boiling point of ~671 ^{o}C it is transferred to the atmosphere in a gaseous form firstly. Once airborne, it cools down, condenses and forms particles that are soluble in water. These particles can be easily transported large distances (more than 1000 km) by wind [18]. A simulation, illustrating the dispersion of ^{137}Cs in the environment, demonstrates the effective proliferation of this radionuclide over vast distances and the contribution to soil and water contamination (Figure 1) [19] [20]. Similarly, especially volatile ^{131}I has a boiling point of ~184 ^{o}C and proliferates easily in a gaseous or aerosol form as well. It has been documented that the incidence of thyroid cancer after the Chernobyl accident increased in population up to 500 km from the accident site [21]. Since the boiling point of ^{90}Sr is ~1382 ^{o}C, it does not tend to form aerosols, but is prone to be transported via particulate matter, alongside other substances, released during accidents [12]. However, the proliferation of these radionuclides depends greatly not only on wind, but precipitation and migration via soil, when they are deposited on land [22].

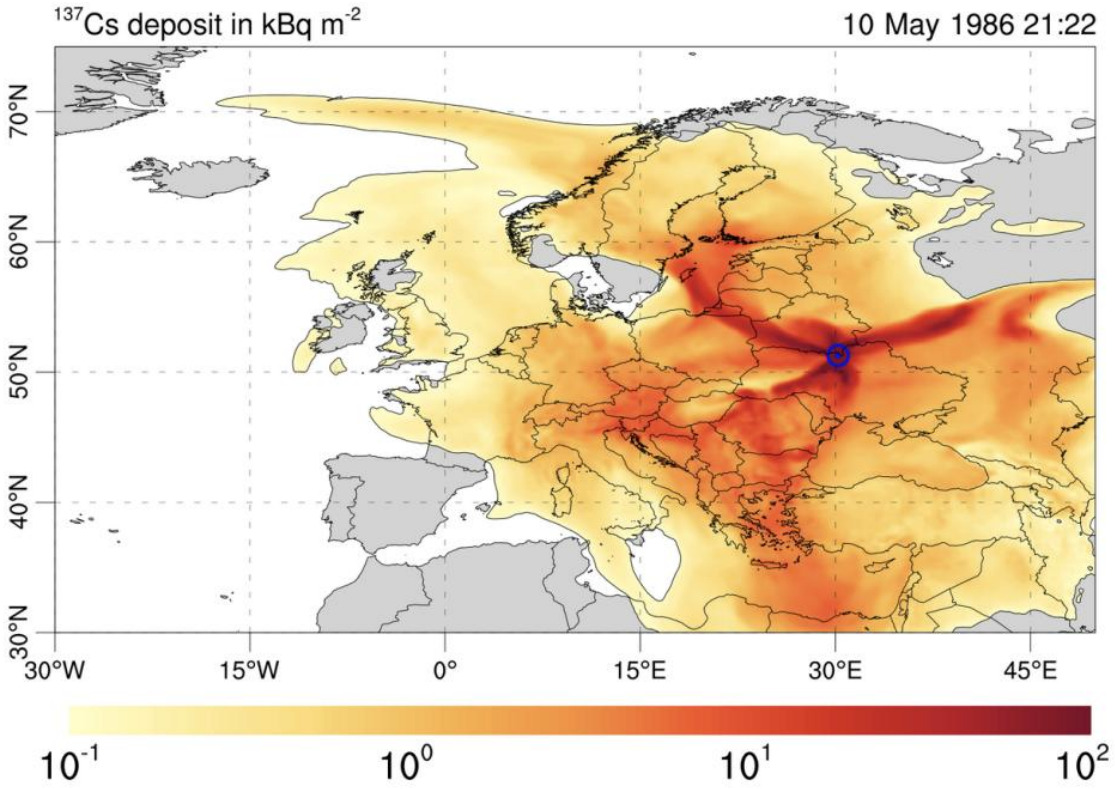

Figure 1. Simulation of Cs-137 distribution in the environment 2 weeks after the Chernobyl accident [20]

1. 2. Radiation interaction with matter

Radiation is divided into two main types: non-ionizing (ultrasound, MRI, etc.) and ionizing, which can further be categorized into directly ionizing (charged particles, like alpha, electrons, ions, hadrons, or neutrons) and indirectly ionizing (neutral particles, like X-rays, gamma rays) [23]. In more detail, alpha particles are positively charged helium nuclei, containing two neutrons and two protons, beta particles can be electrons and positrons, while X-rays and gamma rays are photons – electromagnetic radiation [24]. Even though ionizing radiation can detrimentally affect living organisms, leading to damage at the cellular level (activated cell death, DNA damage like chromosome aberrations or mutations [25]), it has been used for both therapeutic and diagnostic purposes as early as the start of the 20th century, allowing professionals to identify and treat various malignancies [26].

In the case of external radiation exposure, indirectly ionizing radiation, like neutral X-rays or gamma rays, are most dangerous, as they have high penetrability. In addition, higher energy photons require dense materials like lead to be significantly attenuated. Charged particles (electrons, protons, alpha particles or ions) interact with surrounding materials via Coulomb's forces. 5 MeV electrons travel ~17.5 m [27], 5 MeV alpha particles travel ~4 cm in air [28]. The harm to biological tissues also depends a lot on the type of irradiation. That is why different weighting factors are assigned to various irradiations (Table 2).

Table 2. ICRP (2007) radiation weighting factors [29]

Radiation type	**Radiation weighting factor, w_R**
Photons and electrons	1
Protons	2
Alpha particles, heavy ions	20
Neutrons	Continuous function, depending on neutron energy

The degree of interaction can be described by absorbed dose (D), which characterizes the quantity of energy (E_p) deposited per unit mass of matter (m) (Equation 1). Furthermore, equivalent dose (H_T) adjusts absorbed dose, according to the nature of the ionizing radiation (w_R) (Equation 2), and effective dose (E) adjusts equivalent dose, according to the sensitivity of different tissues (w_T) (Equation 3) [29] [30].

$$D = \frac{E_p}{m} \tag{1}$$

$$H_T = \sum_R w_R \cdot D_{T,R} \tag{2}$$

$$E = \sum_T w_T \cdot H_T \tag{3}$$

One of the main emphases of external accidental radiation exposure should be X-rays and gamma rays due to their characteristics, like range in air and penetrability. Gamma rays generally have shorter wavelengths than X-rays, but their energies overlap. The delineation between gamma rays and X-rays is based on the origin of the electromagnetic waves, the former results from nuclear transitions

and the latter results from transitions of electrons in atomic shells or because of slowing of charged particles [31].

It is also important to understand the possible ways photons can interact with matter [28]. There is a number of different photon interactions with matter processes, however in this work only three most important processes will be analyzed (Figure 2):

- **Photoelectric effect** occurs when a photon hits an electron with an energy slightly higher than the binding energy of the inner shell and is completely absorbed. This results in the electron being ejected from the atomic structure. Owing to the vacancy of an electron in one of its orbitals, most often the K shell, the atom is in an excited state. Usually this vacancy is filled by an electron from a higher orbital. During this process a photon is emitted and its energy is equal to the difference in the energies between the two orbital shells. If the emitted fluorescence photon has a high enough energy, it can again ionize a bound electron, resulting in an Auger electron. Both the primary and Auger electrons can deposit energy in matter as well.
- **Compton scattering** occurs when the incident photon interacts with a free electron from the outer shell of an atom and removes an electron from its location. However, during this process the incident photon transfers part of its energy to the electron. The remaining part of photon energy is released in the form of a scattered photon.
- The prerequisite of **pair production** is that the incident photon must have an energy greater than 1.02 MeV, which equals to two electron rest mass energies. During this process the incident photon interacts with the electric field of the nucleus, an electron and positron pair is created. The positron interacts with an electron from another atom and annihilates, releasing two photons of 0.511 MeV in almost opposite directions.

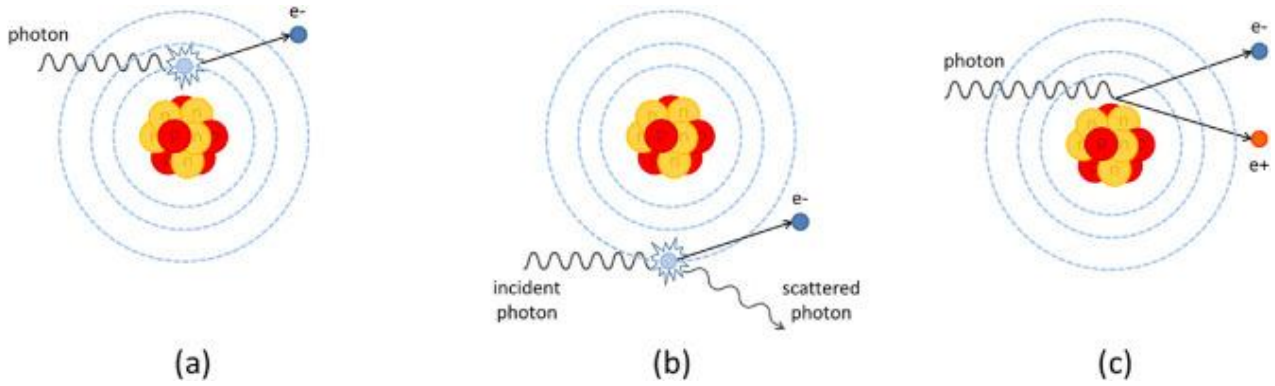

Figure 2. Most significant photon interactions with matter for the scope of this work: photoelectric effect (a); Compton scattering (b); pair production (c) [32]

The probability of these effects mostly depends on the energy of the incident photon and the atomic number of the absorber. For instance, the photoelectric effect is dominant at lower photon energies and higher atomic number of absorber (Figure 3).

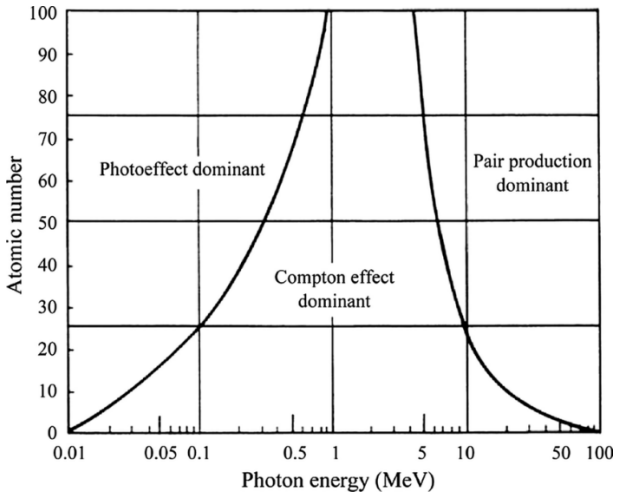

Figure 3. Relative dominance of main photon interactions with matter (adapted from [33])

The information on the indicated processes, also including their probability of interaction via approximate proportionality to photon energy and atomic number of the absorber, is provided in Table 3.

Table 3. Summary of photon interactions with matter [34]

Process	**Type of interaction**	**Variation with photon energy (E)**	**Variation with atomic number (Z)**
Photoelectric	Bound electrons	$\propto 1/E^3$	$\propto Z^3$
Compton scattering	Free electrons	Almost constant 10 – 100 keV; $\propto 1/E$ above 100 keV	Almost independent of Z
Pair production	Promoted by heavy nuclei	Rapid increase above 1.02 MeV	$\propto Z$

1. 3. Radiation detectors and indicators

In this chapter the main radiation detectors and indicators will be discussed in terms of their applicability for the assessment of incident photon exposure.

One promising type of radiation detectors are scintillators. These devices typically have high atomic number elements in their composition, which secure their strong ability to interact with photons, as the increasing density of the material is proportional to larger absorption of photons. Common substances used in scintillation detectors include various iodide salts (sodium, cesium, etc.), doped with tellurium, or various bromide salts, such as lanthanum or cerium bromide. Of course, the usage of these different varieties of materials depends on the specific cases, as they have distinct fluorescence photon emission wavelengths, light yield, energy resolution, and decay times. However, one of the most important issues is the correct light sensor and scintillation crystal combination. It is important, that the wavelength of the fluorescence photons the crystal emits fit with that of the light sensor, because it is sensitive to a certain wavelength of light [35].

The simple working mechanism of these detectors is shown in Figure 4. The interaction of the incident photon with the scintillation crystals (inorganic, organic or gaseous nature) leads to the generation of a number of visible light photons, that are directed to the photomultiplier tube, where they are converted to electrons, and the signal is then multiplied in the dynode network due to an increasing potential between electrodes. The intensity of the measured outgoing signal is proportional to the energy of the incident photon [36].

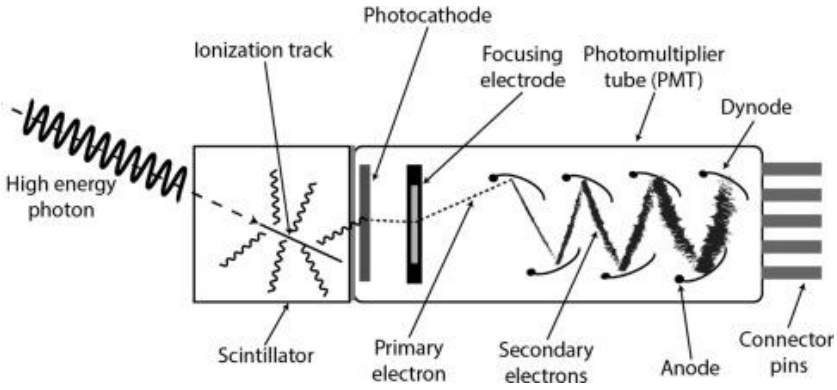

Figure 4. Example of a scintillation detector working mechanism [37]

These scintillation detectors are usually bulky, but recently portable devices, weighing ~200 g only, were developed. A lutetium-yttrium oxyorthosilicate scintillation crystal with a custom readout electronic circuit was designed. However, it still seems quite bulky, cumbersome and of troublesome shape, which could limit it's use also taking into account relatively expensive electronics and uncomfortable donning on clothing [38].

Another type of incident photon radiation detector is based on semiconductors. Similar to materials used in scintillation devices, semiconductor devices also contain high-density elements, such as gallium, silicon, cadmium, telurium, etc. [39]. These detectors are advantageous due to their robustness in harsh environments, like high temperatures and radiation flux [40]. The simple mechanism of a semiconductor detector is associated with the band gap between the valence band, from which electrons can be excited, and the conduction band, to which electrons can be excited. The band gap in insulators is large (≈ 6 eV), while in metals it overlaps. When a semiconductor is doped, for instance, with phosphorus or boron, it is possible to get n- or p-type material respectively. After connecting these electron-rich (n-type) and electron-deficient (p-type) structures and applying an external voltage (usually a reverse bias) to reach an equilibrium state, there will be no flow of charge carriers in the boundary layer. Thus, when an incident photon hits this structure, the equilibrium will be disturbed, more charge carriers will be created (because of photon interactions) and current will be generated, which depends on the energy of the absorbed particles (Figure 5) [41].

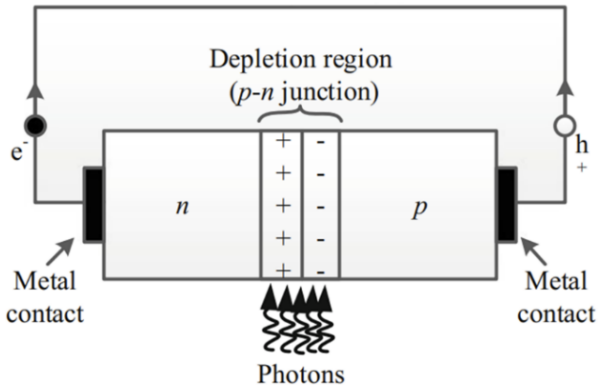

Figure 5. An example of a semiconductor working mechanism (adapted from [42])

Semiconductor devices are promising due to their small size and possible instant exposure assessment (real time data acquisition). However, room temperature operating semiconductor detectors are quite expensive since cadmium, zinc and telurium (CZT) devices require platinum or gold based electrical contacts. Some semiconductor types such as germanium based detectors require liquid nitrogen

cooling to achieve a reduced leakage current, otherwise a significant amount of noise can be registered during operation [43]. Additionally, similar to scintillation detectors, semiconductors also require electronics to read the generated charge, resulting in a bulkier portable gadget [44].

Two other typical detectors used for photon radiation measurements are optically stimulated luminescent (OSL) and thermoluminescent (TLD) dosimeters. However, these two devices require either external light or heat supply to extract radiation exposure data, meaning that other devices are needed. Since these dosimeters are passive, they are not appropriate when assessing and evaluating possible accidental radiation exposure to individuals [45].

Gas filled chambers would also have difficulty being used as portable incident radiation detectors, as they require electrodes, between which a voltage is applied, and other electronic components. Depending on the voltage, gas filled chambers are practically categorized into ionization chambers, proportional region chambers and Geiger Müller counters. Additionally, ionization chambers require large gas volumes to reach high incident particle detection efficiency and greater accuracy [46]. This means that ionization chambers tend to be quite massive. Proportional region chambers require expensive power supplies to keep a stable voltage for the accurate quantification of incident particle energies [47]. Thus, due to expensive electronics, bulky design and necessity for calibration these types of radiation detectors would be impractical as incident radiation detectors, given out to masses of people.

One of the most promising type of dosimeter is chemical-based. Many different compositions are utilized for this purpose. For instance, in Fricke gels radiation induces a color change as a result of the conversion of ferrous (Fe^{2+}) to ferric ions (Fe^{3+}) (Figure 6), while traditional polymer gels rely on polymerization, induced by free radicals after water radiolysis, of monomers in the matrix. Some polymer gels already have a polymer matrix, but rely on additives, such as dyes or other chemicals, which can change color because of redox or bond cleavage reactions. The degree of oxidation, decoloration or polymerization depends on absorbed dose [48]. Of course, there are some problems with chemical dosimeters, especially atmospheric oxygen, which initiates conversion to ferric ions or polymerization of monomers in the absence of ionizing radiation. However, the most common solution for this is the addition of antioxidants or radical inhibitors, such as hydroquinone or various phenols [49] [50]. The dose response of these types of gels can also depend on metal impurities, thus chelators are added like xylenol orange [51]. However, the usual two major advantages of chemical dosimeters are the manufacturing simplicity and the possibility to use relatively cheap radiation sensitive materials. For example, a typical composition of a polymer gel is a gelling agent, monomer, crosslinker and antioxidant. Recently there has been much research in nanoparticle usage in polymer gels, which has been seen to increase the sensitivity of these gels by tens of times [52]. Of course, there are some other disadvantages of chemical dosimeters, primarily being the possible reactivity and toxicity of chemicals used, light sensitivity and limited reusability [53] [54].

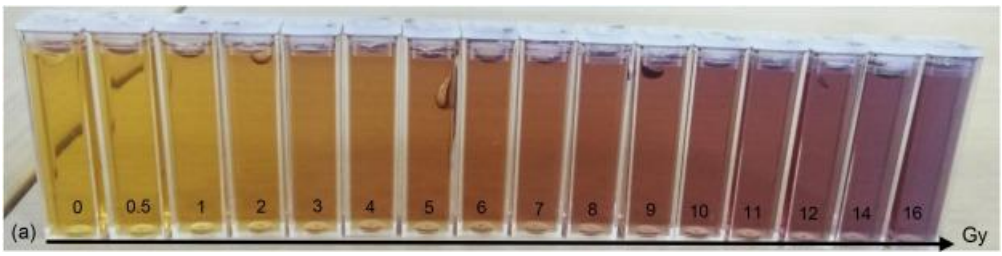

Figure 6. An example of Fricke gel color change after irradiation [55]

1. 4. Typical high dose dosimetry

Various dosimeters can be utilized for radiation exposure measurement. However, most dosimeters are of limitted applicability for the estimation of accidental radiation exposure. For instance, thermoluminescence dosimeters (TLDs) are sensitive to <1 mGy dose [56], but in fact they are not tissue equivalent. Tissue equivalency is important for more accurate representation of radiation impact on biological matter [57], TLDs are passive detectors and require a specific readout procedure (annealing at elevated temperatures [52]), which makes them impractical for accidental radiation exposure detection.

Another important issue with many dosimeters is their sensitivity, as doses that are above 0.2 Gy can result in chronic health-related issues [58] and 50 % lethal dose to population within 30 days of exposure is around 4 Gy [59]. Dosimeters that are based on dyes (Figure 7) typically need large doses to change their optical properties. These dosimeters are based on discolorization (disruption of the conjugated system bonds via oxidation; cleavage of bonds). Authors of the article [60] have shown that the color intensity of indigo carmine dye, having a molar concentration of ~$3.4 \cdot 10^{-5}$ M, was reduced by half after irradiation with ~100 Gy dose, ~730 Gy dose was applied for reactive red 45 ($C_M \approx 6.2 \cdot 10^{-5}$ M) [61] and larger than 7 kGy dose – for reactive blue 19 ($C_M \approx 8.0 \cdot 10^{-5}$ M) [62]. The difference between the doses required to achieve the same discoloration percentage may be associated with the strength and reactivity of the bonds that are most susceptible to oxidation [63].

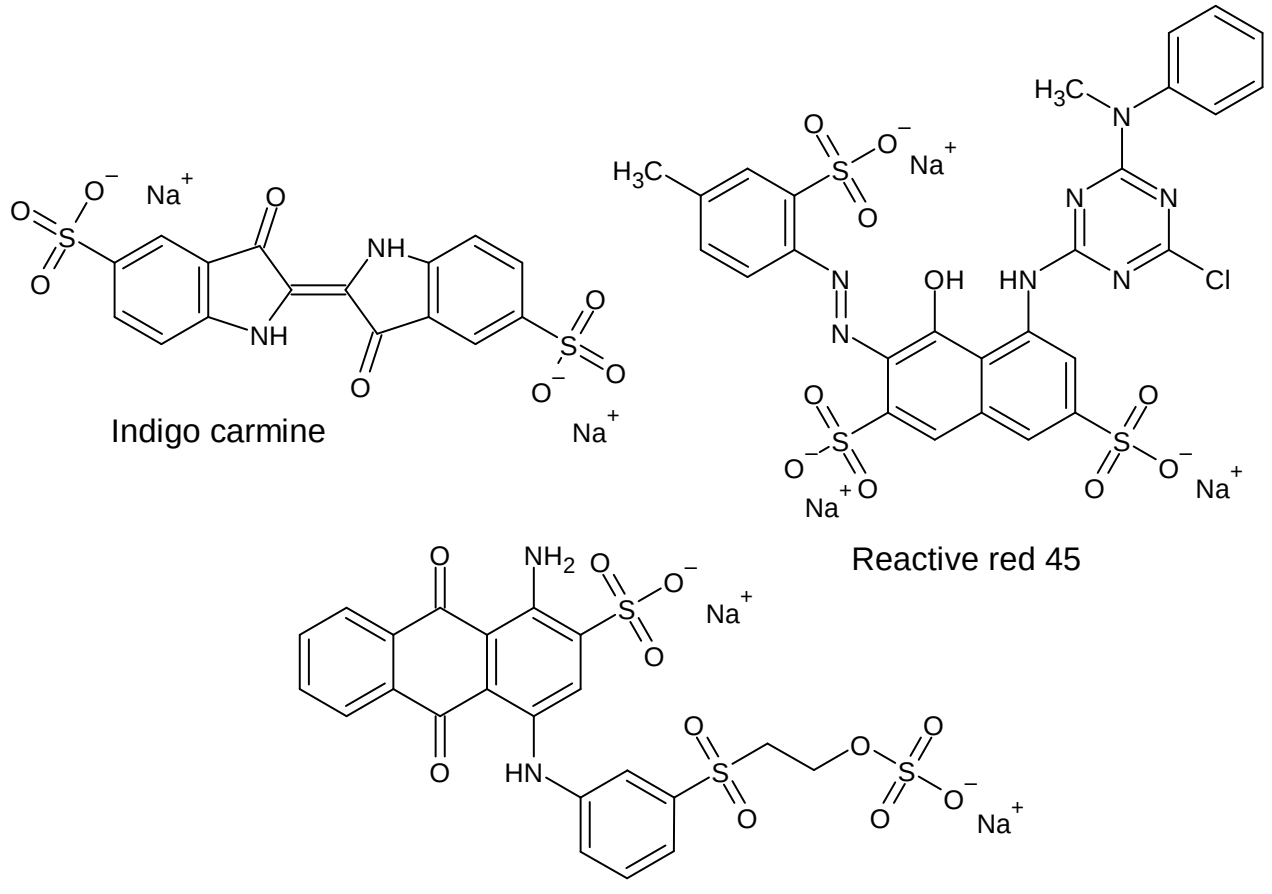

Figure 7. Dyes, which could be used in chemical dosimeters

However, there have been advances with chemical dosimeters that utilize dyes not only as radiosensitive materials, but also as stabilizers. For instance, PRESAGE consists of a clear polyurethane matrix, a radical initiator and radiosensitive materials. This type of dosimeter is still light sensitive and needs to be stored in a dark environment. It has been shown that EBT and PRESAGE films change their color due to exposure to UV-Vis light. The problem was reduced by adding a yellow dye to the composition of EBT2 films, which increased its ambient light resistance as a consequence of the dye's propensity to absorb blue and violet light, which are the most energetic in the visible light spectra [64] [65]. The sensitivity of these types of dosimeters was also inreased, using azo dyes that have reactive and easily cleaved bonds (i.e. R_1-N=N-R_2). Furthermore, azo dyes also act as free radical initiators, further boosting the radiosensitivity. The considered radiochromic plastic dosimeter, consisting of polyurethane matrix, leucomalachite green (as a leuco dye), tetrabromomethane (as a radical initiator) and tartazine (as a yellow dye), significantly changed its optical properties in the dose range of 0.2 – 3 Gy (Figure 8) [66].

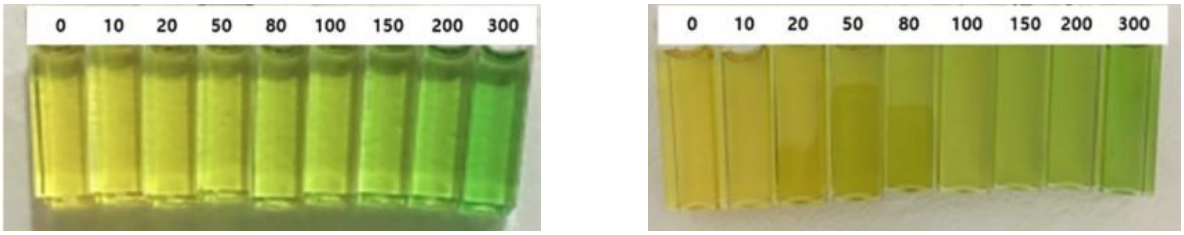

(a) (b)

Figure 8. Modified polyurethane matrix (PRESAGE) dosimeter dose response to gamma irradiation from 0 – 300 cGy: without tartazine (a) and with tartazine (b) [66]

Another azo dye based dosimeter, consisting of poly(vinyl alcohol), silver nitrate nanoparticles (as a radiosensitizer) and nitro blue tetrazolium (NBT) dye was stable under ambient light for up to 30 days, since NBT is yellow in color, which may increase light resistance. This dosimeter was sensitive in the 0 – 20 mGy range, changing its color from yellow to dark brown (Figure 9). The reason for this may be associated with the reduction of NBT dye to formazan, which also causes the formation of hydrazine [67].

Figure 9. Change in the optical characteristics of PVA films, doped with NBT dye [67]

In another experiment PVA was mixed with NBT dye and different nanoparticles (silver and copper(II)). The produced films were irradiated to doses in the range of 0 – 2.6 mGy. It was observed that the addition of silver and copper(II) nanoparticles leads to film color changes even at low irradiation doses, which indicates radiation sensitivity enhancement of irradiated films (Figure 10). Nanoparticles of high atomic number enhance dose sensitivity due to their substantial electron density. It has been seen that such metal nano particle additives can increase radiosensitivity tens of times [52]. The method of action is mostly associated with the higher probability of photoelectric effect, as it increases quickly with the increasing atomic number of the element (Table 3). Thus, as a result of the higher probability of the photoelectric effect, the possibility of primary and Auger electron generation increases, both of which contribute to dose enhancement [68] [69].

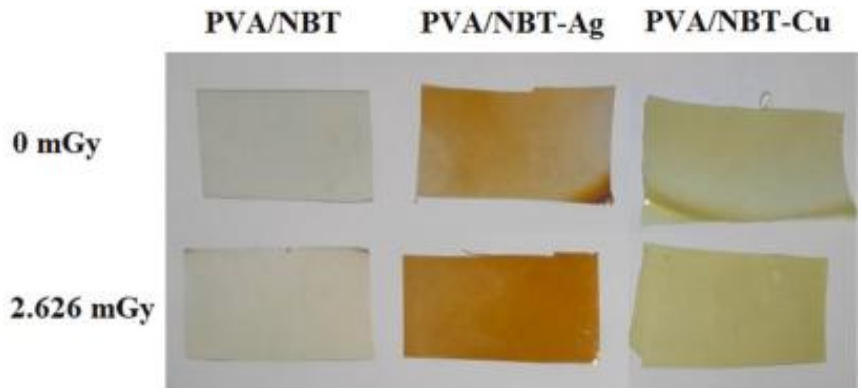

Figure 10. Change in the optical characteristics of PVA-NBT films (adapted from [69])

Another article prepared PVA/NBT films without nanoparticles and irradiated with gamma photons in the dose range of 8 – 96 mGy (Figure 11). It was observed that the color changes were more significant in samples with a higher concentration of the NBT dye, since the color of the films turned brown. This indicates the formation of formazan in the samples, even at low gamma ray doses [70].

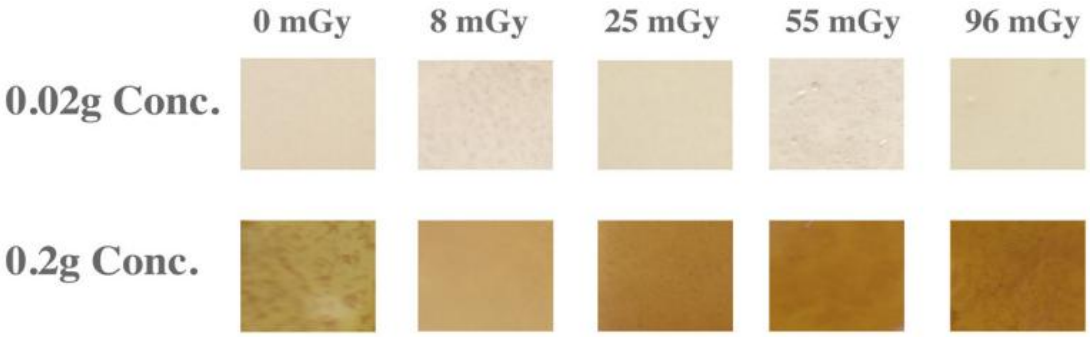

Figure 11. Change in the optical properties of PVA/NBT films, containing differing quantities of NBT dye [70]

Another type of dye that can be added to polymers to indicate the color changes due to photon irradiation is toluidine blue, which is sensitive to UV radiation. It has been observed that a poloxamer 407 hydrogel, containing toluidine blue dye, was bleached when exposed to UV light (Figure 12) [71].

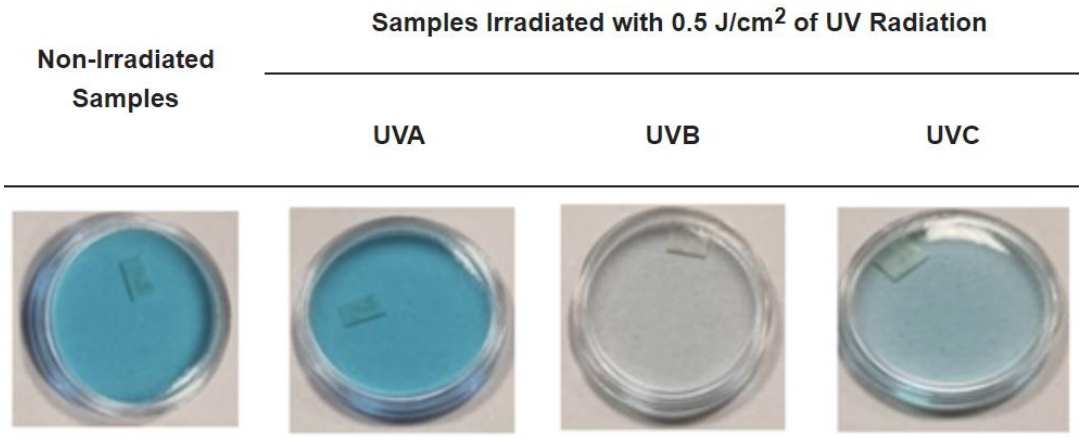

Figure 12. UV light bleaching of Poloxamer 407 hydrogel, doped with toluidine blue (adapted from [71])

The mechanism of action is related to radical induced oxidation of an intramolecular imine, after which the delocalized system is disturbed, leading to bleaching (Figure 13) [71]. Even though the investigated hydrogel was mostly sensitive to UVB light, theoretically it could be adapted as a gamma radiation indicator, as the interaction mechanism is associated with the induced water radiolysis, during which various oxidative species, such as hydrogen and hydroxyl free radicals, hydrogen peroxide and electrons can be formed [72].

Figure 13. Toluidine blue fading reaction [71]

Another type of dosimeter that can alert about gamma radiation exposure is redox reaction based. However, they need high irradiation doses to yield a change in the optical properties. For instance, even though manganese compounds exhibit several colors, starting from pale shades of Mn(II) to black (MnO_2) and to bright hues (Figure 14) [73], kGy range doses are required to facilitate oxidation or reduction to MnO_2 [74] [75].

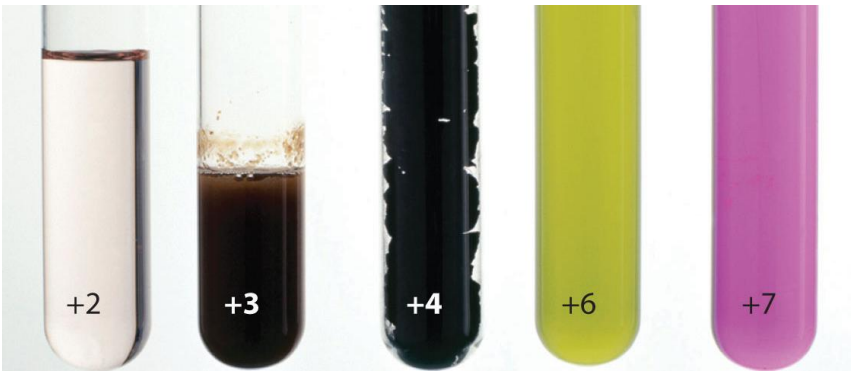

Figure 14. Different colors of manganese compounds at various oxidation states [76]

There have been advances in the redox based reaction dosimeter field recently: fabrication of a novel and reusable colored indicator was proposed, which was sensitive to irradiation doses in the interval of 2 – 8 Gy and was produced without using hazardous chemicals, composing of poly(vinyl alcohol) matrix, iodide and silica nanoparticles [77]. The annealed dosimeter had a white color, which changed to a pale wine red after irradiation, indicating the dependency on the irradiation dose (Figure 15) [78]. The UV-Vis absorption peak, observed at 495 nm, was assigned to the PVA-iodide complex [79]. Researchers also inferred that by attaching silica nanoparticles to the helical structure of PVA an intensification of water radiolysis product generation may be achieved due to charge separation, since pure silicon's atomic structure is an effective semiconductor [77]. The reusability of this dosimeter was also tested by applying irradiation in fractions (8 Gy, 4 Gy and 2 Gy) to reach a total dose of 24 Gy and annealing the indicators after each fraction at 40 ^{o}C for 3 hours. After the irradiation in total with 24 Gy and the final annealing, the color stability was quite good over a 12 day observation period [78].

Figure 15. Color changes of PVA, iodide and silica nanoparticle containing indicator after irradiation to different doses [78]

It has been also found that sensitivity of this detector type can be increased by adding some cross-linkers to the initial composition of the indicator. The authors of the article [80] added the cross-linker glutaraldehyde to PVA-iodide indicator, and irradiated with doses in the range of 0 – 10 Gy (Figure 16). The UV-Vis absorbance peak at 358 nm was analyzed, which was assigned to the presence of free iodide (I_3^-) ions, not bounded to PVA. The sensitivity of PVA-iodine containing radiation indicator was increased by 2.5 times after adding glutaraldehyde as a cross-linker to the composition. It was also found, that these indicators are reusable for at least three times (more than three irradiation and annealing cycles were not performed) [81].

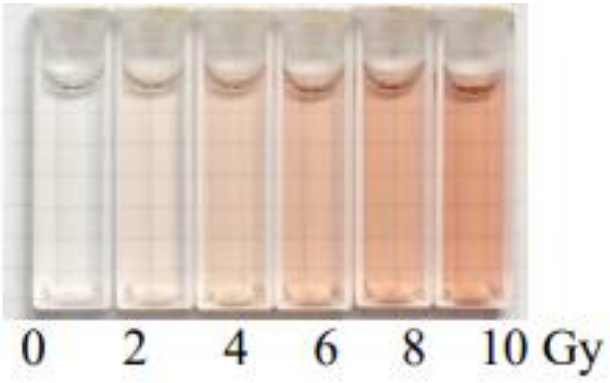

Figure 16. Color changes of PVA-iodide gel, containing glutaraldehyde as a cross-linker after irradiation to different doses [80]

It should be noted that auto-oxidation usually occurs in chemical dosimeters and the PVA-iodide indicators are prone to it as well. The increased stability of these detectors is possible by using free radical scavengers. In a recent study [82] DMSO (dimethyl sulfoxide) was utilized as a stabilizing agent indicating the stability growth with the increased DMSO concentration. Consequently, the radiation sensitivity of the indicator decreased: adding 0.5 M and 1 M of DMSO to the indicators composition led to sensitivity reduction by ~10 % and 18 % respectively. The efforts to adjust the amount of DMSO additive considering the sensitivity-stability relationship led to the conclusion that 0.5 M of DMSO would be optimal [83].

1. 5. Poly(vinyl alcohol) and iodide based chemical dosimeter

Considering the recent advancements in PVA-iodide gels, in this section the radiochemistry of the constituents of this dosimeter type will be briefly explained.

Iodine (I_2) is a chemical element and can be found in nature, especially in marine life, in the form of various salts. At room temperature iodine is a dark-purple crystal, which sublimes to a purple vapor. Iodine has a low solubility in water, but it increases, if there are iodide ions (I^-) in solution. As a result, water-soluble triiodie ions (I_3^-) form. However, many more reactions occur between iodine and water as it can be retrieved from the data provided in Table 4 [84].

Table 4. Main reactions, associated with iodine dissolution in water [84]

Reaction	Reaction type
$I_2 + H_2O \leftrightarrow HOI + H^+ + I^-$	Hydrolysis
$HOI \leftrightarrow OI^- + H^+$	Dissociation
$HOI + H^+ \leftrightarrow H_2OI^+$	Protonation
$I_2 + I^- \leftrightarrow I_3^-$	Complexation
$3HOI \leftrightarrow IO_3^- + 2I^- + 3H^+$	Disproportionation
$I_3^- + I_2 \leftrightarrow I_5^-$	Pentaiodide production
$2I_3^- \leftrightarrow I_6^{2-}$	Dimerization
$OI^- + I^- + H_2O \leftrightarrow HI_2O^- + OH^-$	Disproportionation
$HI_2O^- \leftrightarrow I_2O^- + H^+$	Dissociation

Several UV-Vis absorption (λ) bands are observed for aqueous iodine-iodide solutions. λ_{max} of ~192 nm and ~226 nm peaks represent iodide ions. It is assumed that the absorbance peaks at λ_{max} of ~290 nm and ~360 nm is related to the presence of triiodide ions in the solution (Figure 17). Molecular iodine has a peak at λ_{max} of ~270 nm and solvated iodine molecules – at ~460 nm [85] [86].

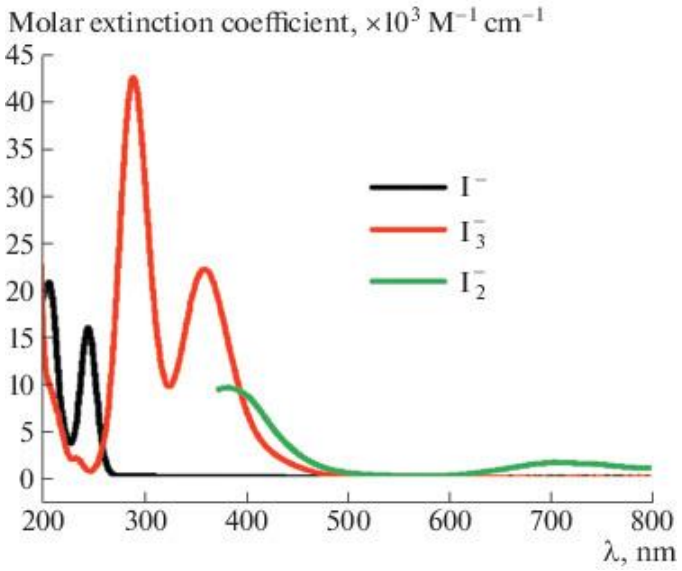

Figure 17. Absorption spectra of iodide, triiodide, and iodine radical anions in acetonitrile [84]

The interaction of iodide species with PVA has also been thoroughly studied. It was suggested that polyiodide ions may penetrate into the interior of the helical PVA molecule aggregates (Figure 18).

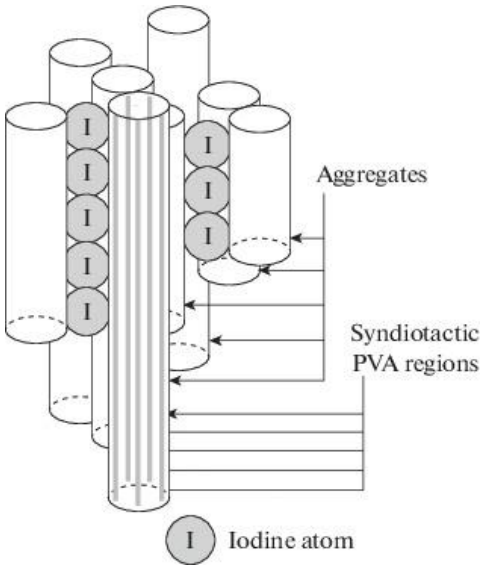

Figure 18. The aggregate model of PVA and iodine complexation [87]

The primary interaction mechanism in a PVA-iodide indicator is related to the oxidation of iodide ions to triiodide or pentaiodide (Figure 19) [88]. The relatively high atomic number of iodine (Z = 53) should be highlighted. It can be inferred that the photoelectric effect and pair production interaction cross-section with gamma rays should be also relatively high.

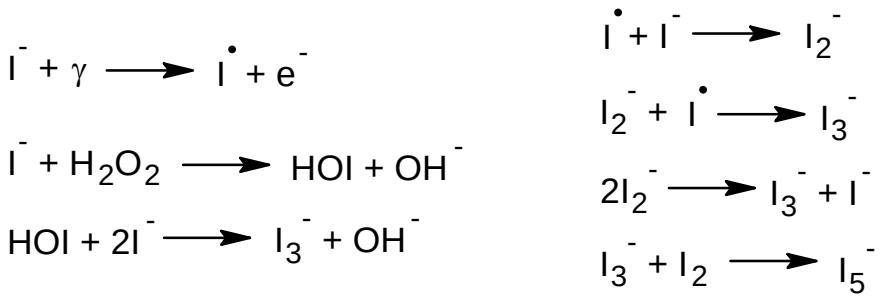

Figure 19. Plausible gamma radiation and iodide species interactions [88]

The enhancement of the yield of polyiodide anions is possible with the utilization of electron scavengers. Even though the reaction kinematics are not entirely understood, it was theoretically assumed that electron scavengers, such as potassium iodate (KIO_3), can interact with electrons creating other reactive species that can oxidize iodide further to polyiodide (Figure 20) [88] [89].

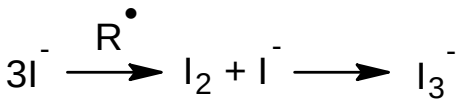

Figure 20. Iodide and reactive species interaction [90]

These polyiodide anions can be complexed by PVA segments. This complexation occurs more readily in amorphous parts of the matrix, even when the concentration of polyiodide anions is quite low, that is why the usage of syndiotactic PVA is more optimal in this case. For this reason, plasticizers, like boronic acid, are used to lower the crystallinity of the PVA matrix.

On the other hand, PVA consists of many hydroxyl groups on the polymer backbone, that can be utilized for chemical modification or even cross-linking [89] [91]. An example of PVA structural changes due to the addition of borax cross-linker is shown in Figure 21 [92]. It has also been observed that PVA-iodide complex has a blue color in the amorphous regions of the PVA matrix, but in high crystallinity regions color can vary from purple to red [93].

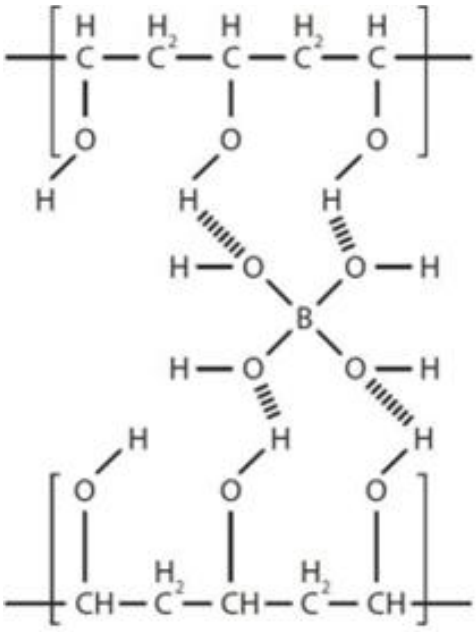

Figure 21. Boronic acid and PVA interlinking mechanism [92]

The authors of the study [91] investigated the diffusion of iodine and potassium iodide solution into a hydrated PVA film. It was observed that the thickness of the hydrated PVA films does not significantly affect the diffusion of iodide ions. It was inferred that iodide ions may be transported via water inside the PVA matrix, as the UV-Vis absorbance of the PVA film samples immediately changed after the injection of iodine and potassium iodide solution. It was also shown that the higher the annealing temperature of PVA was applied, the lower the water permeability and absorption in the matrix was observed. This may indicate molecular structure changes in the PVA matrix related to the creation of stronger intramolecular bonds between the PVA segments, leading to the free space reduction, which can be occupied by water, thus decreasing the degree of PVA hydration. Decreased PVA hydration leads to worse complexation reactions between polyiodide ions and the PVA backbone because of the hindered mobility of polyiodide ions in the matrix itself. However, some complexation is still possible, as in the dry PVA films there is still up to 5 w% of free water remaining that cannot be completely removed under low temperature heat conditions.

To conclude, the main aim of this work is to address the need of immediate monitoring devices (indicators) that could be easily and cheaply manufactured and distributed to the broad public in the case of nuclear accidents or radiological pollution, which otherwise may cause irreversible harm to any living organism. Even though there are numerous advanced radiation detection technologies and equipment, most of them are either expensive, not sensitive enough, or are not able to provide quick and easily understandable information regarding environmental contamination, such as color changing indicators.

The aim of this work was to develop a PVA based hydrogel, sensitive to low dose (<10 Gy) photon irradiation.

The following tasks were set to implement this aim:

1. to develop polymer-based radiation indicators containing iodine;
2. to evaluate changes in the optical properties of fabricated radiation indicators, irradiated with X-ray photons in the 0.2 Gy – 10 Gy dose range;
3. to assess the dose sensitivity of fabricated radiation indicators, according to the variations in their optical properties after irradiation.

2. Materials and methods

Two types of experimental samples (solid films and liquid state samples) of PVA based radiation indicators, containing different concentrations of potassium iodate (KIO_3), potassium iodide (KI), sodium tetraborate ($Na_2[B_4O_5(OH)_4]\cdot 8H_2O$), and glycerol ($C_3H_8O_3$) were fabricated. Composition of the prepared films and solutions are provided in Table 5.

Table 5. Chemical composition of experimental samples

Experimental samples		**H_2O, w%**	**KIO_3, w%**	**KI, w%**	**$Na_2[B_4O_5(OH)_4]\cdot 8H_2O$, w%**	**$C_3H_8O_3$, w%**	**PVA(20 % solution), w%**
Films	F1	-	5	20	0.4	1	73.60
	F2	20	0.45	2	0.08	0.5	76.97
Solutions	S1						
	S2	20	-	2	0.08	0.5	77.42
	S3	20	-	5	0.08	0.5	74.42

Potassium iodide (KI, purity ≥99.5 %), potassium iodate (KIO_3, purity ≥99.5 %), sodium tetraborate ($Na_2[B_4O_5(OH)_4]\cdot 8H_2O$, purity ≥99.5 %), and glycerol ($C_3H_8O_3$, purity ~96 %) were purchased from Eurochemicals GmbH, Nordgorn, Germany, for fabrication of the experimental samples, as well as polyvinyl alcohol ($(C_2H_4O)_n$, M_w ~125000 MOWIOL® 20-98 MW) was purchased from Sigma-Aldrich Chemie GmbH, Germany, analytic-grade water for laboratory use (H_2O) was purchased from Chempur Piekary Śląskie, Poland. Standard PMMA UV-Vis cuvettes (Sigma-Aldrich Chemie GmbH, Germany) were used for filling of experimental solutions.

2.1. Preparation of samples – radiation indicators

Experimental films. A 20 % water solution of PVA was used for preparation of the experimental samples. It was prepared in a beaker, mixing 20 g of PVA powder with 80 g of distilled water under continuous stirring at elevated temperature of 70 ^oC for approximately 60 minutes in a Steinberg Systems (Berlin, Germany) SBS-MR-1600/1T PRO magnetic stirrer until a homogeneous solution was achieved.

For the preparation of the F1 (5 w% KIO_3) film solution a mixture of 6 g of potassium iodide, 1.50 g of potassium iodate and 0.12 g of sodium tetraborate were ground in a mortar with a pestle to powder. The powder was added to a beaker with 22.08 grams of 20 % stock PVA solution and 0.30 g of glycerol dissolved at 40 ^oC. The total mass of the prepared film solution was ~30 g. The beaker with the prepared PVA stock solution and glycerol was wrapped with aluminum foil to minimize interaction with ambient light and air. Glycerol additive was used to increase the malleability, flexibility, and viscosity of the polymer gels [94]. The solution was mixed under continuous stirring until homogeneity was achieved. The prepared solution was immediately poured into 60 x 15 mm Petri dishes (Figure 22) and left to dry for 12 h at 40 ^oC, while ensuring a dark environment. 10 g of prepared solution was used for fabrication of each film sample, that were ~1 mm thick after drying.

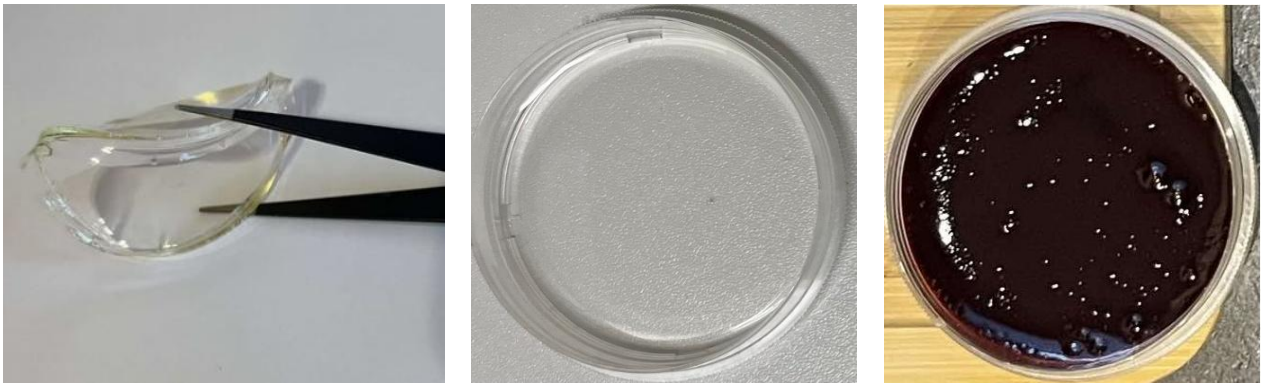

(a) (b) (c)

Figure 22. Photographs of the dried pure PVA films (a,b) and F1 film (c) in Petri dishes

F2 (0.45 w% KIO_3) films were prepared from 1.000 g of potassium iodide, 0.225 g of potassium iodate, 0.040 g of sodium tetraborate, and 0.250 g of glycerol dissolved in 10 g of distilled water at room temperature. Prepared salt solution was slowly poured into 38.485 g of 20 % PVA stock solution at 40 ^oC. The total mass of the prepared solution was approximately 50 g. The beaker with the film solution was wrapped with aluminum foil. The solution was continuously mixed at a constant RPM until a homogeneous solution was prepared (approximately 30 minutes). The mixed solution was poured into 60 x 15 mm Petri dishes and left to dry for 12 h at 40 ^oC, while ensuring a dark environment. 7 g of the prepared solution was used to form ~0.8 mm thick films after drying. Color changes of the experimental solutions were observed almost immediately after their fabrication (Figure 23).

(a) (b) (c)

Figure 23. Photographs of F2 (0.45 w% KIO_3) film solution 15 minutes post preparation (a); 2 hours post preparation (b); after drying (c)

Experimental solutions. The preparation procedure of the S1 (0.45 w% KIO_3) indicator solution was identical to that of F2 (0.45 w% KIO_3) film solution. To form the liquid indicator, 3.5 g of the prepared solution was poured into 12.5 x 12.5 x 45 mm PMMA cuvettes (1.25 mm wall thickness), ensuring a dark environment during their storage. The cuvettes were also covered with Parafilm to avoid excessive interaction with air (Figure 24).

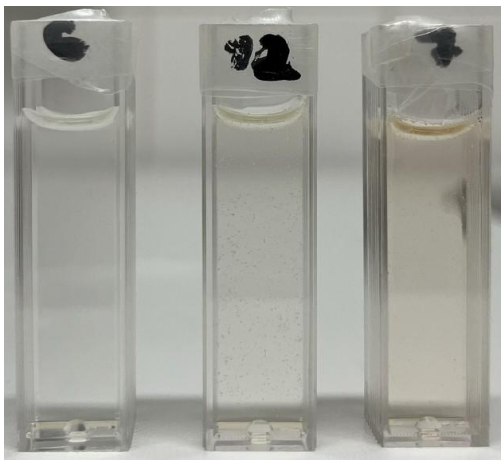

Figure 24. From left to right: pure PVA solution; S1 (0.45 w% KIO_3) solution 5 minutes post preparation; S1 (0.45 w% KIO_3) solution 15 minutes post preparation

The preparation procedure of the S2 (2 w% KI) indicator solution (Figure 25) was identical to the S1 (0.45 w% KIO_3) indicator solution, but without adding potassium iodate to the composition. 1.00 g of potassium iodide, 0.04 g of sodium tetraborate, and 0.25 g of glycerol dissolved in 10 g of distilled water at room temperature were used to prepare the salt solution, which was slowly poured into 38.71 g of 20 % PVA stock solution at 40 ^{o}C and mixed. The total mass of the prepared film solution was approximately 50 g.

Figure 25. From left to right: pure PVA solution and S2 (2 w% KI) solution 7 days after preparation

The preparation procedure of the S3 (5 w% KI) indicator solution (Figure 26) was identical to the S2 (2 w% KI) indicator solution, only the mass of potassium iodide was increased to 2.50 g and the prepared salt solution was poured into 37.21 g of 20 % PVA stock solution at 40 ^{o}C. The total mass of the prepared film solution was also approximately 50 g.

Figure 26. From left to right: pure PVA solution and S3 (5 w% KI) solution 7 days after preparation

2.2. Irradiation of samples

Prior to irradiation, the experimental F2 films were cut into (1.75 x 1.75) cm^2 squares.

Irradiation of experimental samples (film squares and cuvettes with experimental solutions) with 6 MeV X-ray photons was performed in linear accelerator Clinac DMX (Varian Medical Systems, Inc., USA) at the Oncology Institute of the Lithuanian University of Health Sciences (Figure 27). The dose rate of 600 MU/min was used for irradiation of samples with the doses from the interval of 0.2 – 10 Gy. The source-to-surface distance (SSD) was kept at 100 cm for all irradiations, while the gantry angle of 180º and field size of 30 x 30 cm^2 was used. The dose delivered to the films was verified with 0.6 cm^3 sensitive volume PTW (Freiburg, Germany) Farmer TM30013 ionization chamber

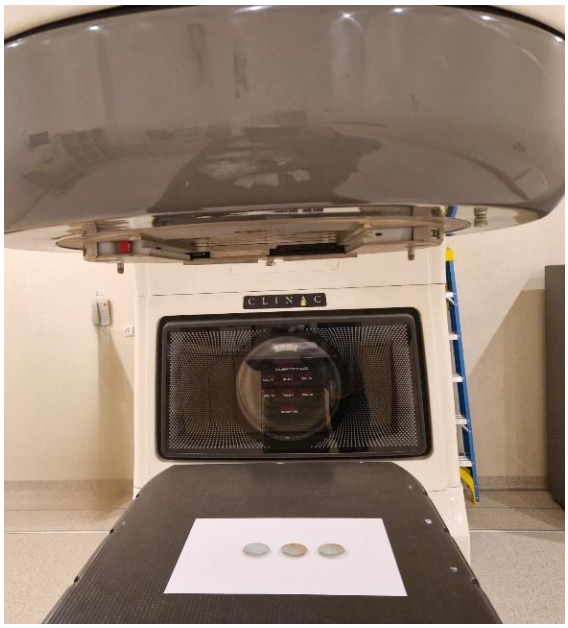

Figure 27. Irradiation geometry of experimental films

Irradiation of F1 films was not performed at all, since highly inhomogeneous structure of films was obtained due to the incompatibility of the relatively large concentration of potassium iodate with potassium iodide.

2.3. Analytical techniques and characterization of the experimental samples

UV-Vis spectroscopy method is based on the electronic transitions in the material when UV-Vis beam crosses it. This method can be used to study transition metal complexes (due to d and f electrons), unsaturated conjugated organic compounds, and organic compounds, containing heteroatoms (oxygen, nitrogen, iodine, etc.). Usually near-UV region (200 – 370 nm) and the visible region (380 – 700 nm) are used [95] and the light intensity change after crossing the material follows the Beer-Lambert law (Equation 4).

$$I = I_0 \cdot 10^{-\varepsilon c l} \tag{4}$$

where I is the transmitted intensity, a.u.; I_0 is the incident intensity, a.u.; ε is the extinction coefficient (molar absorptivity, color intensity), L/(mol·cm); c – solution concentration, M; l – path length of the cuvette, cm.

Optical density (absorbance A) is equal to the base-10 logarithm of the ratio of the initial light intensity (I_0) to the light intensity after passing through the sample (I) (Equation 5) [96].

$$A = \lg\left(\frac{I_0}{I}\right) \tag{5}$$

If the extinction coefficient is very low, electronic transitions do not occur – only forbidden transitions take place (Equation 6) [97].

$$A = \varepsilon c l => \varepsilon = \frac{A}{cl}, \tag{6}$$

Absorbance can be converted to transmission (T) by using the relationship in Equation 7 [95].

$$A = -\log_{10} T \tag{7}$$

Pre-irradiation and post-irradiation analysis of the optical properties of the experimental films and solutions was performed using spectrometer Ocean Optics with USB4000 (Ocean Optics, Inc., Dunedin, Fl, USA) with a light source HL-2000-LL by Ocean Insight (Figure 28). Ocean View spectroscopy software (version 1.6.7 by Ocean Optics) was used for the result analysis [98]. Changes of the optical properties were evaluated using common methodology [99]. The calibration of the spectrometer was performed in air, whereas the UV-Vis spectra of the PMMA cuvette filled with water was used for the reference data. The sensitivity of the films and solutions was attained analyzing the UV-Vis spectra, and was based on the dose response curve to absorbance measured at characteristic wavelengths.

Figure 28. Fiber optic spectrometer Ocean Optics (left) and light source HL-2000-LL (Ocean Insight) (right)

3. Results and discussion

3.1. Characterization of experimental films – radiation exposure indicators

The intension for preparing F1 (5 w% KIO_3) film type indicators was to ensure that the maximum possible amount of additives would dissolve in the 20 % PVA stock solution. The solubility of potassium iodate is only ~6.5 % [100], sodium tetraborate ~3.7 % [101], while potassium iodide has a quite large solubility ~58.9 % [102]. Three obstacles were identified performing this experiment: 1) as soon as potassium iodide and potassium iodate were mixed with PVA, the red PVA-triiodide complex was formed because of oxidizing potassium iodide to polyiodide species by potassium iodate; 2) due to the large amount of sodium tetraborate and insufficient mixing speed, hardened sections of the cross-linked PVA-borate structures were formed, preventing homogeneity; 3) the water amount in the 30 g of 20 % PVA solution of F1 (5 w% KIO_3) was ~14.7 g, while the amount of water needed to dissolve 6 g of potassium iodide is ~4.2 g, 1.5 g of potassium iodate ~21.6 g and 0.12 g of sodium tetraborate ~3.1 g, making request for ~28.9 g of water in total. Theoretically these salts should also be dissolved by glycerol and especially the PVA itself, as it comprises of a lot of acetyl- and hydroxyl (polar) groups. Even though the dissolution process was quite complicated, no undissolved salts were visually seen. Further investigation of this film's radiation sensitivity related to color changes upon irradiation was impossible due to very intense dark red color of the solution (Figure 22 (c)). The most important take away from this experiment was that too large of an amount of potassium iodate cannot act as a sensitizer, but rather it interacts with potassium iodide as an oxidizer. It was also found that the concentration of sodium tetraborate should be reduced as the cross-linked PVA-borate structure became too difficult to manage. Lastly, the amount of 1 w% of glycerol in the solution is too high since it decelerates drying of the films.

Preparation and investigation of F2 (0.45 w% KIO_3) films was performed with the intention to ensure the applicability of PVA-iodide films containing potassium iodate as a sensitizer for the indication of radiation exposure. The most important challenge related with this experiment was associated with the quick cross-linking of the prepared potassium iodide, potassium iodate, glycerol and sodium tetraborate solution (the salt solution) with the PVA matrix in the stock solution. The problem was alleviated by adding the prepared salt solution in small portions and ensuring sufficient mixing of the PVA solution. Another well known problem was related to the slow yellowing of the salt solution as a result of the potassium iodate interaction with potassium iodide to form various iodide species. It was found that the produced film solution initially was colorless, but started to turn lightly pinkish within 15 minutes following the sample preparation and became red after a few hours (Figure 23). The main takeaway from this experiment was that potassium iodate is seemingly incompatible in these types of PVA gels as a consequence of its highly oxidative nature.

Since water content plays a crucial role for the properties of PVA based films, swelling-deswelling behaviour of pure 20 % PVA films was compared with that of F2 (0.45 w% KIO_3) films (Table 6). It is important to note that PVA_1 and PVA_2 films were not completely dry in this experiment. Since a lesser amount of PVA was used to form F2 (0.45 w% KIO_3) films, a larger percentage amount of water was evaporated during the drying process, because less water was coordinated and hydrogen bonded to a smaller amount of PVA [91]. Another important finding was that the red color, most likely formed due to PVA-triiodide complexation, disappeared following water evaporation. Red color incrementally changed to yellow in dried F1 (5 w% KIO_3) and F2 (0.45 w% KIO_3) films probably because of potassium iodate oxidation of potassium iodide to iodide species (Figure 23).

The later findings led to suggest that larger amount of water is required in order to form the red PVA-triiodide complex [91].

Table 6. Swelling and deswelling of pure 20 % PVA matrix and F2 films

Type of film	Mass of film solution, g	Mass of film, g	Evaporated mass, g	Initial water content in film solution, g	Percentage of evaporated water, %
PVA_1	7	1.85	5.15	5.6	92.0
PVA_2		1.84	5.16		92.1
PVA_3		1.64	5.36		95.7
PVA_4		1.62	5.38		96.1
PVA_5		1.62	5.38		96.1
PVA_6		1.65	5.35		95.5
F2_1		1.4	5.6	5.71	98.0
F2_2		1.4	5.6		98.0
F2_3		1.46	5.54		97.0
F2_4		1.42	5.58		97.7
F2_5		1.44	5.56		97.3

The feasibility of fabricated iodine containing PVA films to serve as radiation exposure indicators was assessed, analyzing F2 (0.45 w% KIO_3) films irradiated to different X-ray doses in a linear accelerator. Since the dried films were already yellow, indicating possible presence of different iodide species in the film, color changes of these films after irradiation were expected. However, no significant color changes were found when inspecting irradiated films visually (Figure 29).

Figure 29. Photographs of F2 (0.45 w% KIO_3) films, irradiated to different doses

The UV-Vis spectroscopy may provide some information regarding color changes of the objects that cannot be identified by visual inspection of samples. It is known, that pure PVA has absorbance peaks at 280 nm and 335 nm [103], iodate ions (IO_3^-) have an absorbance peak at ~180 nm, iodine (I_2) has an absorbance peak of ~203 nm, and triiodide ions (I_3^-) have absorbance peaks of ~288 nm and ~350 nm [104]. In the study, which investigated PVA and potassium iodide films, an absorbance maximum of ~255 nm was observed, intensity of which was increasing with the increased concentration of KI in the films [105]. Lastly, the PVA-triiodide absorbance peak is at ~490 nm [89] [106].

Prior to starting analyzing the UV-Vis spectra of experimental F2 (0.45 w% KIO_3) films and of pure PVA (Figure 30), it is to state that there was no possibility to identify peak locations of iodate ions (IO_3^-) and iodine (I_2) if any, due to the limited wavelength range of the available spectrometer.

Analysis of the obtained UV-Vis spectra revealed that the absorption properties of pure PVA indicated slightly increasing tendency with the increasing dose, which could be followed by observing absorption peaks at ~280 nm and ~335 nm. This minimal increase of absorption can be attributed to possible polymer structure changes upon irradiation. On the contrary, UV-Vis light absorption by PVA containing films 0.45% of KIO_3 (F2 film) is higher as compared to pure PVA and increases

more significant upon irradiation. Due to the small amounts of different species, a high UV-Vis absorption in the broad wavelength range of ~280 nm to 420 nm is observed indicating restructurization of polymer matrix due to additives and due to irradiation. The characteristic peak at ~490 nm related to the PVA-triiodide complex was also not visible.

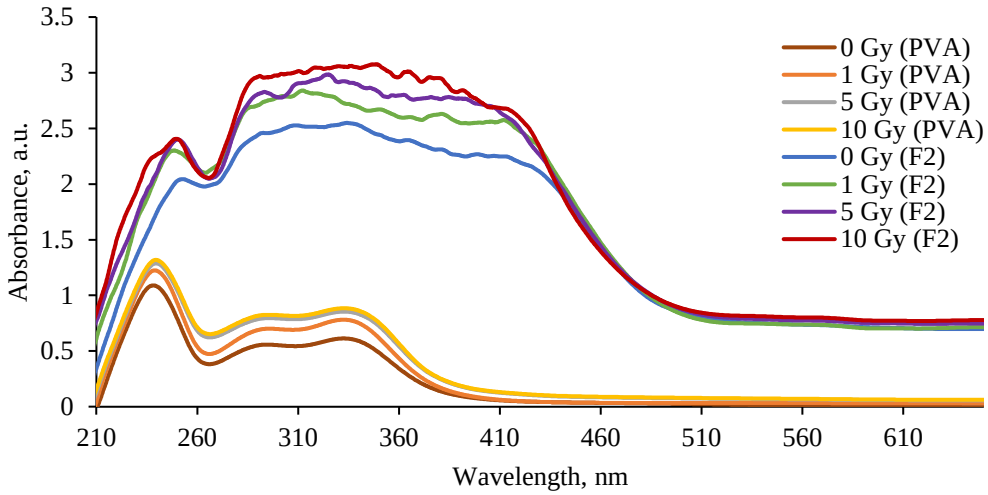

Figure 30. Absorbance UV-Vis spectra of PVA and F2 (0.45 % KIO_3) films

3.2. Characterization of liquid radiation indicators

The intention for preparation of S1 (0.45 w% KIO_3) indicator solution was verification of the water importance for the formation of the PVA-triiodide complex. The S1 (0.45 w% KIO_3) indicator solution behaved similarly to F1 (5 w% KIO_3) and F2 (0.45 w% KIO_3) films: initial solution was colorless, but started to redden, even in a completely dark environment (Figure 24). The red color became more intense within the next few days (Figure 31) and did not disappear during long term storage or after irradiation. The takeaway from this experiment was similar as in the case of F1 (5 w% KIO_3) and F2 (0.45 w% KIO_3) films – due to the highly oxidative nature of potassium iodate, it is seemingly incompatible in these types of PVA indicator solutions.

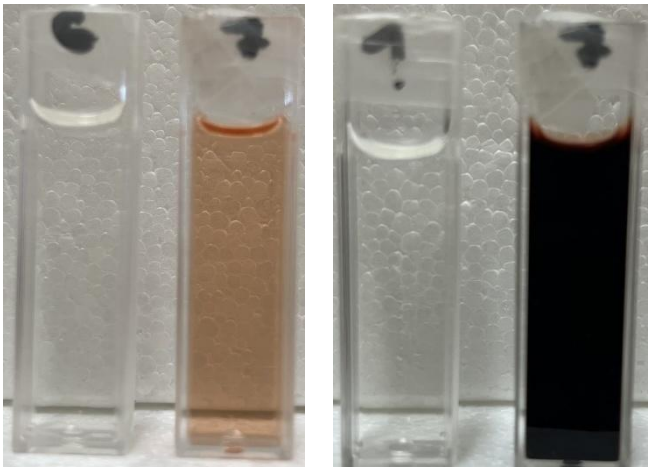

(a) (b)

Figure 31. Photographs of pure PVA solution and S1 (0.45 w% KIO_3) solution 2 hours post preparation (a); pure PVA solution and S1 (0.45 w% KIO_3) solution 7 days post preparation (b)

The intention for fabrication of S2 (2 w% KI) indicator solution was verification of the negative effect of potassium iodate on the auto-formation of PVA-triiodide complex. It was observed that the salt solution started to become slightly yellow before adding it to the PVA matrix. This may be because of the auto-oxidation of potassium iodide, as a consequence of interacting with light and air. This process may be mitigated by adding the salt solution to the PVA matrix as fast as possible, while also trying to maintain a dark environment. It was found that the prepared S2 (2 w% KI) indicator solution was colorless even 7 days after preparation (Figure 25). It did not turn red or even yellow. This behavior can be related to the viscosity of the PVA matrix solution and proper Parafilm sealing of the filled cuvettes, that prevent interaction of the excess air with the potassium iodide in the experimental solution.

The intention for fabrication of S3 (5 w% KI) indicator solution was radiation sensitivity enhancement of the solution. To mitigate the yellowing of the salt solution, at first sodium tetraborate and glycerol were dissolved in water at room temperature and the beaker was covered with aluminum foil to avoid ambient light. Only afterwards was the potassium iodide dissolved at room temperature and the prepared salt solution was immediately poured into the 20 % PVA matrix solution. The beaker with the prepared solution was covered with aluminum foil as well. Unlike the S2 (2 w% KI) indicator solution, the initially colorless S3 (5 w% KI) indicator solution turned slightly red within 7 days after preparation (Figure 26). This process may be mitigated by adding radical scavengers such as DMSO, as it was proposed in the literature review [83]. It would also be possible to reduce coloring of the solution by varying concentration of potassium iodide, which might be between 2 w% and 5 w%. The sensitivity of this liquid radiation indicator could also be increased utilizing sensitizers like high atomic number salts (for instance, silver nitrate) [94].

Optical properties of experimental samples were investigated analyzing UV-Vis spectra of the indicator solutions. Figure 32 shows UV-Vis transmittance spectra of PVA and S1 (0.45 w% KIO_3) indicator solutions. It was found, that PVA absorbs light in the ~250 – 340 nm wavelength range like expected. However, analyzing UV-Vis transmittance in S1 indicator 2 hours after sample preparation (S1; 2 h), very distinct PVA-triiodide peak ~490 nm was observed, which indicates that potassium iodate present in the solution oxidized potassium iodide to triiodide species and the PVA-triiodide complex was formed. It was impossible to identify any spectral peaks in S1 (0.45 w% KIO_3) solution 7 days after preparation (S1; 7 d), because of the intense dark red color.

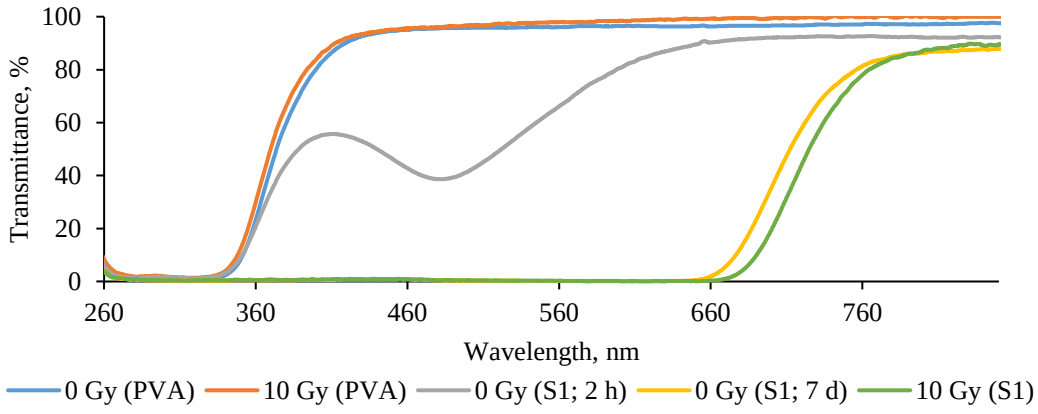

Figure 32. UV-Vis transmission spectra of PVA and S1 (0.45 w% KIO_3) indicator solutions, where 0 Gy (S1; 2h) indicates S1 solution spectrum 2 h after preparation and 0 Gy (S1; 7 d) – 7 days after preparation

Due to the initial deep red color of samples before irradiation, it was not possible to distinguish any color changes of irradiated samples visually as well (Figure 33).

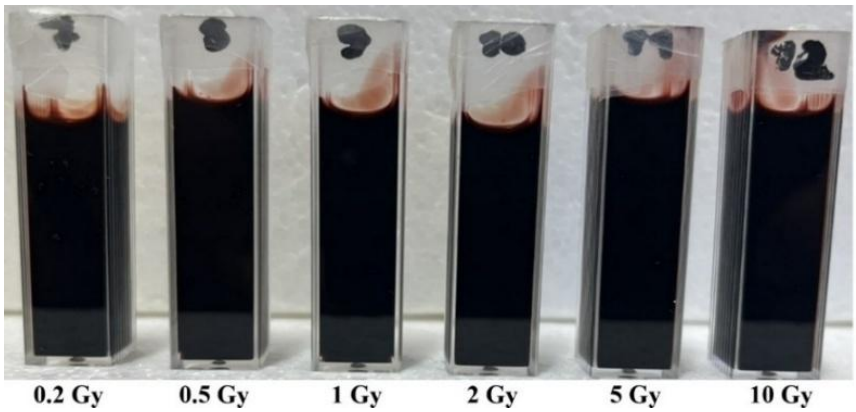

Figure 33. Photograph of color of S1 (0.45 w% KIO_3) indicator solution after irradiation to different doses

Characteristic UV-Vis absorption/transmission peak related to PVA-triiodide complex can be seen in Figure 34 for S2 (2 w% KI) and S3 (5 w% KI) indicator solutions after their irradiation to 10 Gy dose. The corresponding peak at ~490 nm can be seen more easily in the transmission spectra, where ~10 % intensity decrease for the S2 (2 w% KI) and ~30 % intensity decrease for the S3 (5 w% KI) can be observed after irradiation of samples.

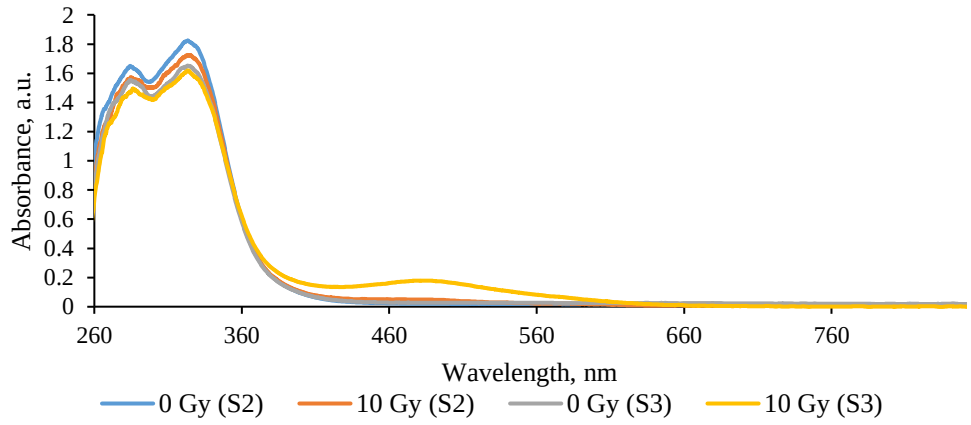

(a)

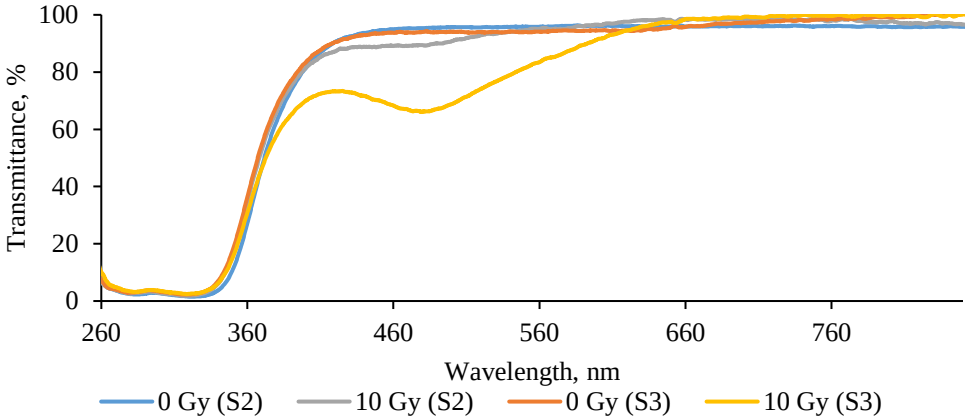

(b)

Figure 34. UV-Vis absorption (a) and UV-Vis transmission (b) spectra of initial not irradiated and irradiated to 10 Gy dose S2 (2 w% KI) and S3 (5 w% KI) indicator solutions

Figure 35 shows relevant UV-Vis transmission fragments of S2 (2 w% KI) indicator solutions after irradiation of samples to various doses (a) and repeated irradiation with the same doses (b).

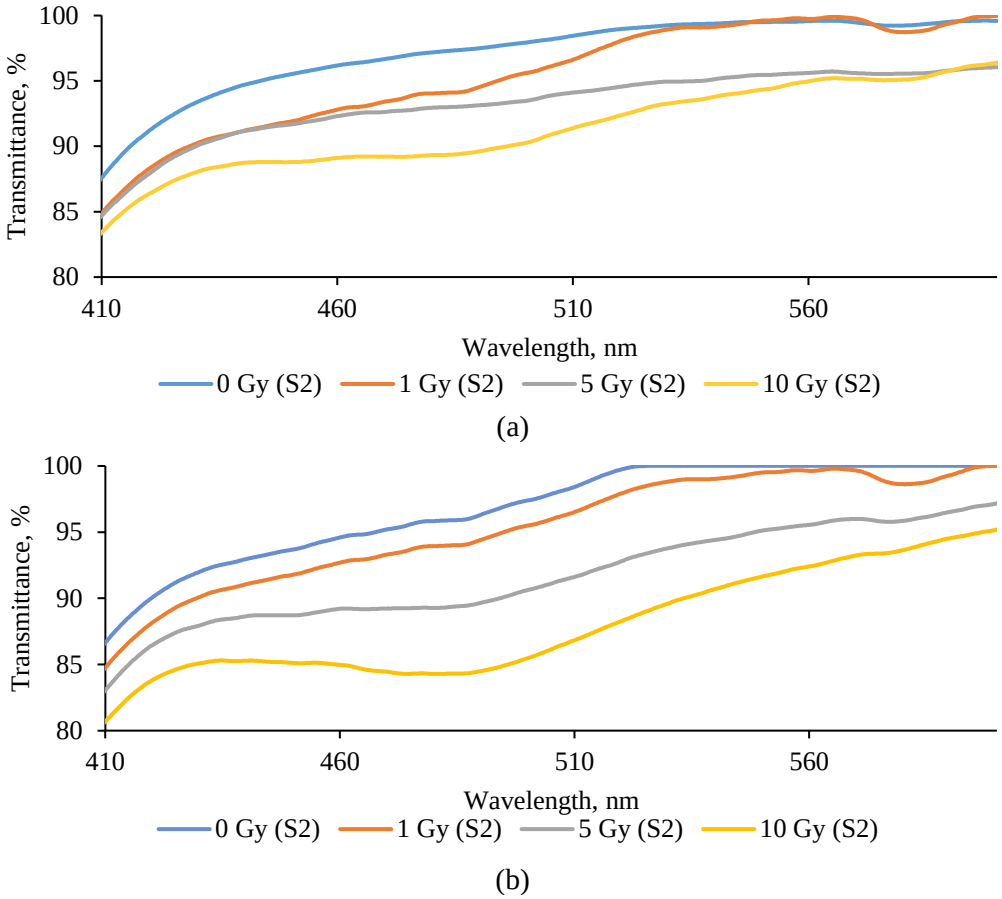

Figure 35. Fragments of UV-Vis transmission spectra of S2 (2 w% KI) solution after the first round of irradiation (a), and after the second round (b) of sample irradiation with the same doses

It should be noted that S2 (2 w% KI) indicator solutions were quite insensitive to ambient light and air conditions during irradiation and UV-Vis analysis procedures, as there was no PVA-triiodide related peak in the transmission spectra even 7 days after sample preparation. After the first irradiation round of the S2 (2 w% KI) indicator solutions, they became clear after an additional week in dark storage. After the second irradiation round with the same doses some more significant visual color changes were observed (Figure 36).

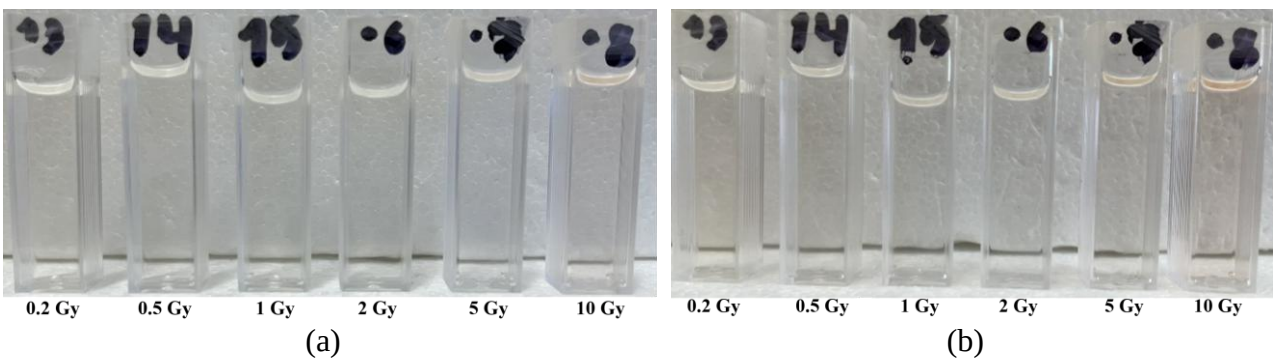

Figure 36. Photographs of the color changes of S2 (2 w% KI) indicator solutions after first irradiation cycle (a) and after second irradiation cycle (b)

UV-Vis transmission spectra of S3 (5 w% KI) indicator solution is shown in Figure 37, which indicates the higher dose sensitivity of S3 samples compared with S2 (2 w% KI) indicator solutions.

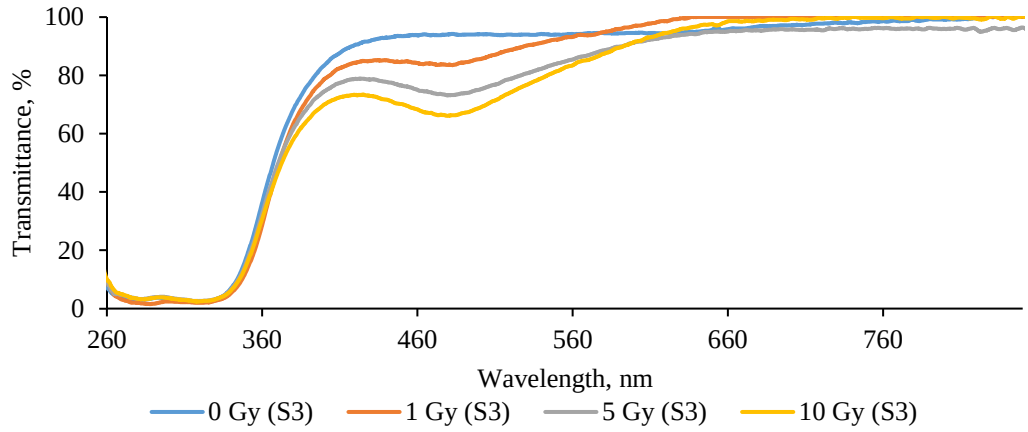

Figure 37. UV-Vis transmission spectra of S3 (5 w% KI) indicator solution samples

However, the auto-oxidation of potassium iodide to polyiodide species contributes to dose related reduction of transmission intensity, which could be observed at the characteristic PVA-triiodide complex peak at ~490 nm wavelength. This can be observed also in Figure 38, which shows photographs of S3 solutions irradiated to different doses, where the initial not irradiated solution (left most) was already reddish, indicating increased instability, most likely attributed to the increased potassium iodide concentration in the solution.

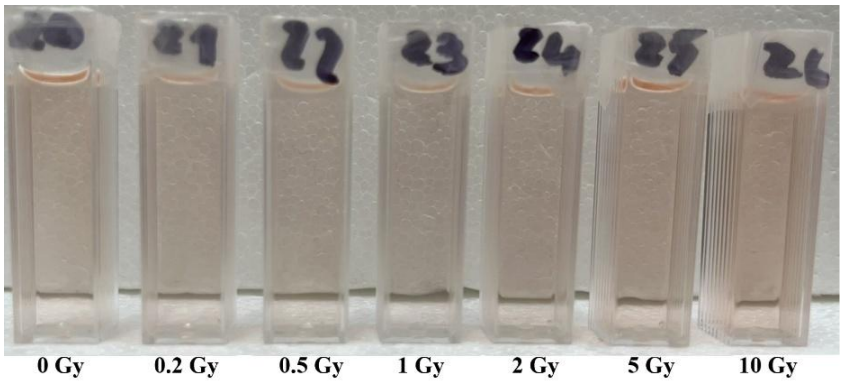

Figure 38. Photograph of color changes of S3 (5 w% KI) indicator solution samples

This feature may be utilized searching for the most favorable potassium iodide concentration, corresponding to the highest radiation sensitivity, while remaining stable after minimal exposure to ambient light.

Obtained UV-Vis absorbance spectra of irradiated S3 (5 w% KI) radiation indicators were very similar to those provided by other authors for similarly composed samples [89]. Comparison of UV-Vis absorbance spectra fragments with indicated absorbance peak at ~490 nm related to the formed PVA-triiodide complex for both indicators is provided in Figure 39.

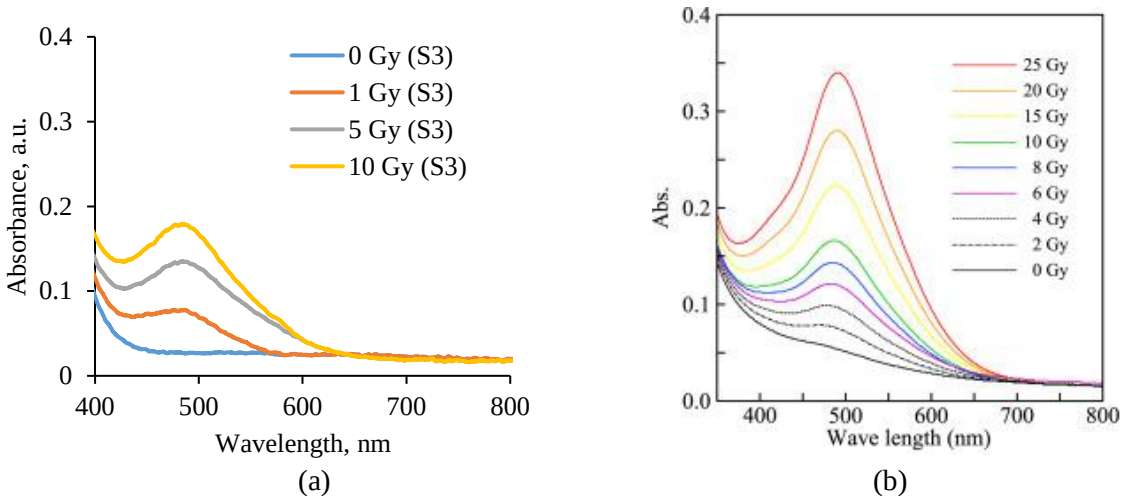

Figure 39. Comparison of the UV-Vis absorption spectra fragments: irradiated S3 indicator solution (a) and irradiated PVA + Gellan Gum + KI + Fructose gel (b) [89]

Since evaluation of occasional exposure indicated by radiation indicators may be postponed due to field conditions, follow up of their optical properties was performed, comparing UV-Vis spectra of S1 (0.45 w% KIO_3), S2 (2 w% KI) and S3 (5 w% KI) indicator solutions immediately after irradiation and one month after irradiation (Figure 40). It is to note that all samples before and after irradiation were were kept in a dark and dry environment.

Analysis of the spectra led to the conclusion that irradiated S1 (0.45 w% KIO_3) samples were oxidized even further, as the transmission started to increase at a longer wavelength. This may be explained due to the oxidation of potassium iodide to a larger variety or concentration of iodide species, for instance, pentaiodide (I_5^-). Furthermore, PVA-pentaiodide absorbance maximum is at 645 nm versus the 490 nm absorbance maximum, corresponding to the PVA-triiodide complex [91] [107].

As for the S2 (2 w% KI) samples, it can be seen that after one month some transmission increase was observed, especially at ~490 nm, which corresponds to PVA-triiodide characteristic peak. This is in line with the previous results, where the red color of the samples diminished with time due to the reductive capabilities of the polyiodide ions to iodide ions [89].

At 5 w% potassium iodide concentration in indicator solution S3, sample oxidization proceeded further as significantly higher PVA-triiodide complex absorption peak at ~490 nm was observed after one month.

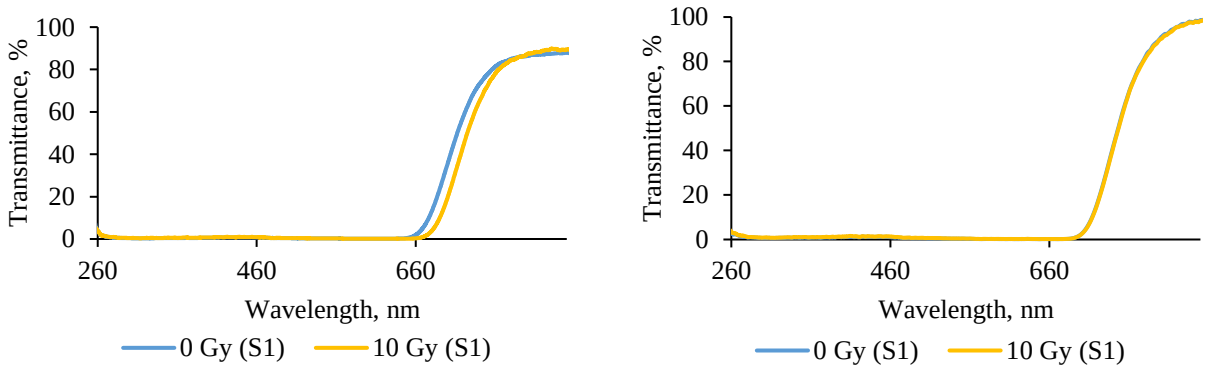

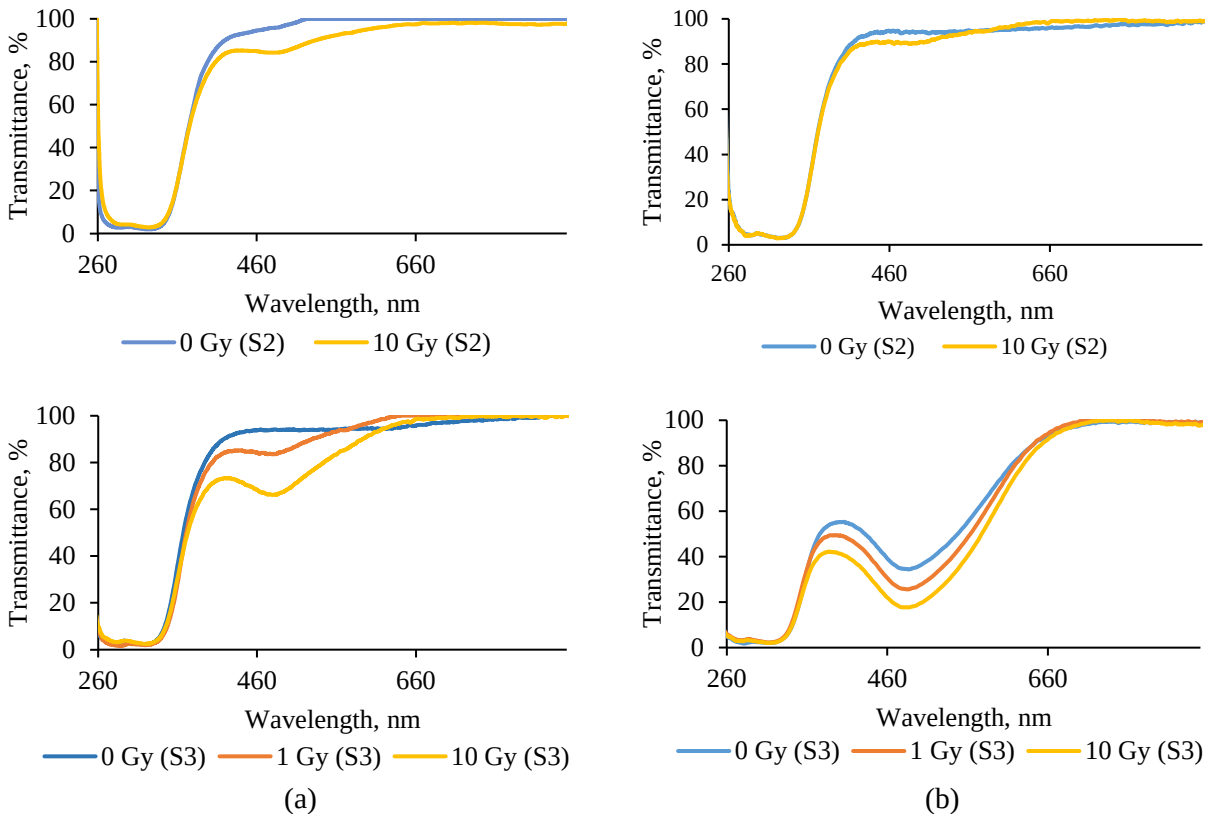

Figure 40. UV-Vis transmission spectra of S1, S2 and S3 indicator solution samples: immediately after irradiation (a) and one month after irradiation (b)

3.3. Sensitivity of the developed radiation indicators

Radiation sensitivity of irradiated samples was evaluated as a slope of the dose response curve to the optical properties changes of samples.

Performed investigation revealed that radiation sensitivity of the produced F2 (0.45 % KIO_3) films is relatively low (0.0429 Gy^{-1}) (Figure 41). It is to suggest that the composition of the PVA-iodine based experimental films needs to be adjusted for better color changes and higher radiation sensitivity prior to exploring them as radiation exposure indicators.

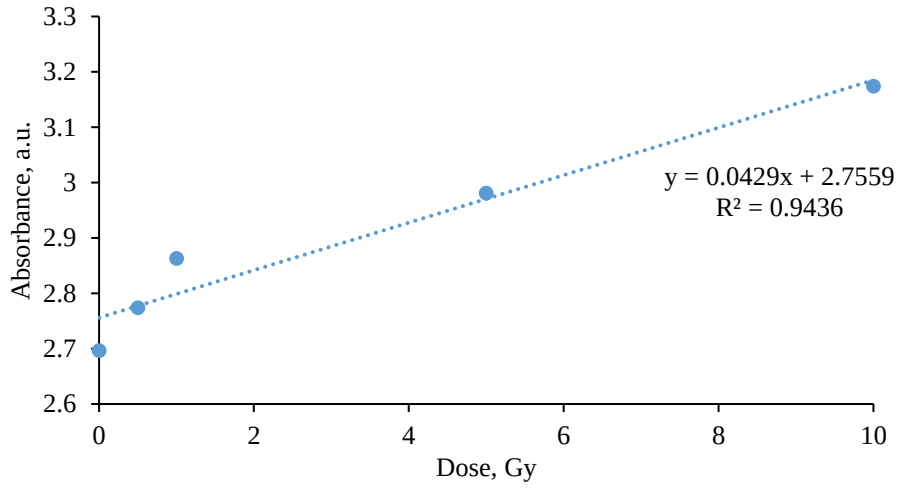

Figure 41. Dose response curve to UV-Vis absorbance changes (at ~340 nm) of F2 (0.45 w% KIO_3) film samples

Radiation sensitivity of S1 samples was not evaluated because of their color changes to deep red almost immediately after preparation. It was also impossible to distinguish optical changes after sample irradiation with different doses (Figure 33). Dose response curves to UV-Vis absorbance changes for the S2 (2 w% KI) and S3 (5 w% KI) indicator solutions are shown in Figure 42. Obtained sensitivity values were detectable, however very small: 0.0058 Gy^{-1} and 0.0135 Gy^{-1} for S2 and S3 correspondingly.

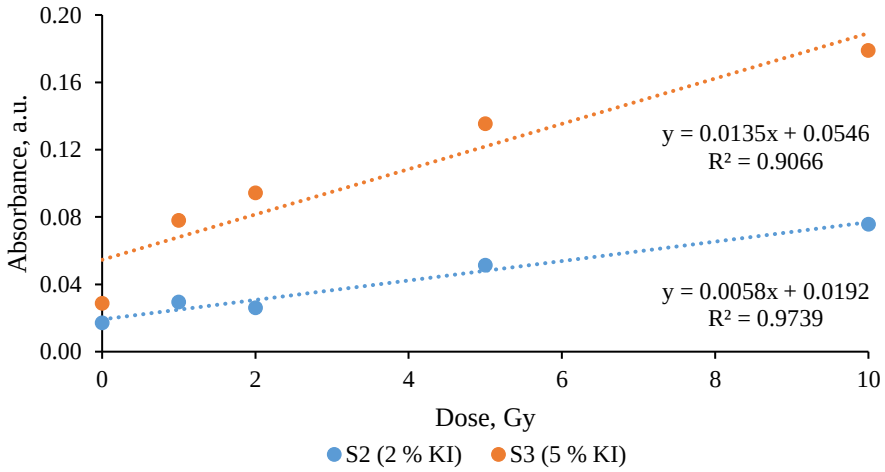

Figure 42. Dose response curves to UV-Vis absorbance changes (at ~490 nm) of S2 (2 w% KI) and S3 (5 w% KI) indicator samples

It is to point out, radiation sensitivity of S3 (0.0135 Gy^{-1}) was similar to that provided by other authors (0.010 Gy^{-1}) [89] as it can be retrieved from Figure 39b.

Conclusions

Promising PVA-iodide based radiation exposure indicators are proposed in this work, that change their optical properties from a clear solution to a faint red color in the dose range of 0 – 10 Gy. Gels of this PVA-I type offers advantages such as simplicity, portability and cost-effectiveness. However, additional experiments must be performed to ensure a better sensitivity to radiation and more resistance to ambient conditions, such as light and temperature.

1. Two batches of films and three batches of indicator solutions, containing different concentrations of potassium iodate, potassium iodide, sodium tetraborate, glycerol and 20 % PVA, were prepared. The purpose of F1 films, which had very high concentrations of the salts (5 w% potassium iodate, 20 w% potassium iodide, 0.4 w% sodium tetraborate, 1 w% glycerol), was to ensure that the maximum possible amounts of chemicals would dissolve in the 20 % PVA stock solution. The salts ostensibly dissolved, but the resulting films were inhomogeneous due to problematic mixing. F2 films had a lower concentration of salts (0.45 w% potassium iodate, 2 w% potassium iodide, 0.08 w% sodium tetraborate, 0.5 w% glycerol), but this time it was concluded that potassium iodate is seemingly incompatible in these types of PVA gels due to its highly oxidative nature. The same conclusion was reached with S1 indicator solution, which had the same salt amount. S2 indicator solution, which had the same salt amount as F2 films and S1 indicator solution, but without potassium iodate, was the most stable of the experiments (no color change due to ambient conditions), but was not as sensitive. S3 indicator solution, which had a similar composition to S2 indicator solution, but more potassium iodide (5 w% versus 2 w%), was the most sensitive of the experiments, but not as stable (PVA-triiodide complex formed without irradiation).
2. F1 films were unirradiated, because of their inhomogeneity. F2 films a few hours after preparation turned red and after drying – yellow, but the color after irradiation did not seem to significantly change. S1 solution also a few hours after preparation turned red and after a few days – dark red; the color after irradiation did not seem to significantly change as well. S2 solution was colorless and only changed color to a pale red, when irradiated with 5 Gy and 10 Gy. S3 solution turned a slight red in the 7 days post preparation, but the color change after irradiation increased with dose, most distinctly seen with 5 Gy and 10 Gy dose samples. The PVA-triiodide peak at ~490 nm was present in the UV-Vis transmission spectra of S1 – S3 solutions. When a follow up after one month post irradiation of the indicator optical properties was performed, S1 samples were oxidized even further, S2 samples had a reduction in the PVA-triiodide peak (due to reductive properties of iodide species) and S3 samples were oxidized even further (higher absorbance at PVA-triiodide peak).
3. The dosimetric sensitivity was not done for F1 films, because of their inhomogeneity. The sensitivity of F2 films, according to the ~340 nm absorbance maximum of triiodide ions, was only 0.0429 Gy^{-1}. According to the ~490 nm absorbance maximum of PVA-triiodide complex, S2 indicator samples had a sensitivity of 0.0058 Gy^{-1} and S3 indicator samples had a sensitivity of 0.0135 Gy^{-1}, which was comparable to a similar composition indicator sensitivity (0.010 Gy^{-1}), described in literature.

List of references

1. IAEA. *IAEA Safety Standards for protecting people and the environment General Safety Guide No. GSG-7 Occupational Radiation Protection Jointly sponsored by* [online]. 2018. [Accessed 20 April 2025]. Available from: http://www-ns.iaea.org/standards/
2. TALAPKO, Jasminka, TALAPKO, Domagoj, KATALINIĆ, Darko, KOTRIS, Ivan, ERIĆ, Ivan, BELIĆ, Dino, VASILJ MIHALJEVIĆ, Mila, VASILJ, Ana, ERIĆ, Suzana, FLAM, Josipa, BEKIĆ, Sanja, MATIĆ, Suzana and ŠKRLEC, Ivana. Health Effects of Ionizing Radiation on the Human Body. *Medicina 2024, Vol. 60, Page 653* [online]. 18 April 2024. Vol. 60, no. 4, p. 653. [Accessed 6 February 2025]. DOI 10.3390/MEDICINA60040653. Available from: https://www.mdpi.com/1648-9144/60/4/653/htm
3. WANG, Kaikai, ZHANG, Wei, QI, Yameng, HU, Xiaodan, ZHANG, Xiaohong, CHANG, Shuquan and ZHANG, Haiqian. Radiation-sensitive nanogel-incorporated Fricke hydrogel dosimeters with reduced diffusion rates. *Polymers for Advanced Technologies* [online]. 1 February 2023. Vol. 34, no. 2, p. 539–548. [Accessed 20 April 2025]. DOI 10.1002/pat.5904. Available from: https://onlinelibrary.wiley.com/doi/full/10.1002/pat.5904
4. HU, Naonori, NAKAMURA, Taiki, KATAURA, Ryusuke, SUGA, Keita, MUKAWA, Tetsuya, AKITA, Kazuhiko, SASAKI, Akinori, NOJIRI, Mai, MATSUBAYASHI, Nishiki, TAKATA, Takushi, TANAKA, Hiroki, NIHEI, Keiji and ONO, Koji. Implementation of optically simulated luminescent dosimeter for quality control of gamma ray dose of an accelerator-based neutron source. *Journal of Applied Clinical Medical Physics* [online]. 1 November 2024. Vol. 25, no. 11, p. e14493. [Accessed 20 April 2025]. DOI 10.1002/acm2.14493. Available from: https://onlinelibrary.wiley.com/doi/full/10.1002/acm2.14493
5. VAN BLAADEREN, J. Jasper, VAN AARLE, Casper, LEIBOLD, David, DORENBOS, Pieter and SCHAART, Dennis R. *Guidelines for the Selection of Scintillators for Indirect Photon-Counting X-ray Detectors* [online]. 2025. American Chemical Society. [Accessed 20 April 2025]. Available from: https://pubs.acs.org/doi/full/10.1021/acs.chemmater.4c03437
6. ADLIENE, Diana, URBONAVICIUS, Benas Gabrielis, LAURIKAITIENE, Jurgita and PUISO, Judita. New application of polymer gels in medical radiation dosimetry: Plasmonic sensors. *Radiation Physics and Chemistry*. 1 March 2020. Vol. 168, p. 108609. DOI 10.1016/J.RADPHYSCHEM.2019.108609.
7. ZHANG, Ping, JIANG, Li, CHEN, Hong and HU, Liang. *Recent Advances in Hydrogel-Based Sensors Responding to Ionizing Radiation* [online]. 12 April 2022. Multidisciplinary Digital Publishing Institute. [Accessed 22 May 2024]. Available from: https://www.mdpi.com/2310-2861/8/4/238/htm
8. FEHNER, Terrence R and GOSLING, F G. *Origins of the Nevada Test Site*. 2007.
9. YAKUBU, A, DARMA, TH, IBRAHIM, UM and MAITAMA, A. Assessing Ionizing Radiation Exposure Risks to Human Health in Wadi-B, Jere Oil Exploration Areas, Borno State, Nigeria. *researchgate.net* [online]. 2024. Vol. 4. [Accessed 15 February 2025]. Available from: https://www.researchgate.net/profile/Tijjani-Darma/publication/384821657_Assessing_Ionizing_Radiation_Exposure_Risks_to_Human_Health_in_Wadi-B_Jere_Oil_Exploration_Areas_Borno_State_Nigeria/links/678f9ba075d4ab477e53e021/Assessing-Ionizing-Radiation-Expos
10. IAEA. *IAEA SAFETY STANDARDS for protecting people and the environment Radiological Monitoring for Protection of the Public and the Environment* [online]. 2023. [Accessed 15 February 2025]. Available from: https://www.iaea.org/sites/default/files/24/01/draft_ds505.pdf
11. MINISTRY OF THE ENVIRONMENT GOVERNMENT OF JAPAN. Booklet to Provide

Basic Information Regarding Health Effects of Radiation (4th edition). [online]. 2024. Vol. 1, p. 266. [Accessed 22 February 2025]. Available from: https://www.env.go.jp/en/chemi/rhm/basic-info/1st/pdf/basic-1st-vol1.pdf

12. KOARAI, Kazuma, KINO, Yasushi, OKA, Toshitaka, TAKAHASHI, Atsushi, SUKZUKI, Toshihiko, SHIMIZU, Yoshinaka, CHIBA, Mirei, OSAKA, Ken, SASAKI, Keiichi, URUSHIHARA, Yusuke, FUKUDA, Tomokazu, ISOGAI, Emiko, YAMASHIRO, Hideaki, FUKUMOTO, Manabu, SEKINE, Tsutomu and SHINODA, Hisashi. Incorporation and Accumulation of Strontium-90 in the Hard Tissue of Animals and Their Relationship with Strontium-90 Pollution in the Environment. *Low-Dose Radiation Effects on Animals and Ecosystems: Long-Term Study on the Fukushima Nuclear Accident* [online]. 1 January 2019. P. 53–62. [Accessed 22 February 2025]. DOI 10.1007/978-981-13-8218-5_5/FIGURES/3. Available from: https://link.springer.com/chapter/10.1007/978-981-13-8218-5_5
13. IIZUKA, Kazuya, TOYA, Narumi, OHSHIMA, Jyunichi, ISHIGURI, Futoshi, MIYAMOTO, Naoko, AIZAWA, Mineaki, OHKUBO, Tatsuhiro, TAKENAKA, Chisato and YOKOTA, Shinso. Relationship between 137Cs concentration and potassium content in stem wood of Japanese cedar (Cryptomeria japonica). *Journal of Wood Science* [online]. 1 February 2018. Vol. 64, no. 1, p. 59–64. [Accessed 22 February 2025]. DOI 10.1007/S10086-017-1673-9/FIGURES/4. Available from: https://jwoodscience.springeropen.com/articles/10.1007/s10086-017-1673-9
14. AGENCY FOR TOXIC SUBSTANCES AND DISEASE REGISTRY. Health effects of Cesium-134 and Cesium-137. In : [online]. 2003. [Accessed 22 February 2025]. Available from: https://www.atsdr.cdc.gov/toxprofiles/tp157-c3.pdf
15. Application Nucléide – Lara – Laboratoire National Henri Becquerel. [online]. [Accessed 22 February 2025]. Available from: http://www.lnhb.fr/accueil/donnees-nucleaires/module-lara/
16. KELLEHER, Kevin. Radiation Monitoring in Ireland – The Impact and Lessons Learned from Nuclear Accidents. *Radiation Environment and Medicine* [online]. 2017. Vol. 6, no. 2, p. 49–54. [Accessed 22 February 2025]. Available from: https://www.jstage.jst.go.jp/article/radiatenvironmed/6/2/6_49/_pdf/-char/ja
17. FDA. *Xenon gas for diagnostic use* [online]. 2011. [Accessed 22 February 2025]. Available from: https://www.fda.gov/drugsatfda
18. WAI, Ka Ming, KRSTIC, Dragana, NIKEZIC, Dragoslav, LIN, Tang Huang and YU, Peter K.N. External Cesium-137 doses to humans from soil influenced by the Fukushima and Chernobyl nuclear power plants accidents: a comparative study. *Scientific Reports 2020 10:1* [online]. 13 May 2020. Vol. 10, no. 1, p. 1–8. [Accessed 22 February 2025]. DOI 10.1038/s41598-020-64812-9. Available from: https://www.nature.com/articles/s41598-020-64812-9
19. KOARASHI, Jun, NISHIMURA, Syusaku, ATARASHI-ANDOH, Mariko, MUTO, Kotomi and MATSUNAGA, Takeshi. A new perspective on the 137Cs retention mechanism in surface soils during the early stage after the Fukushima nuclear accident. *Scientific Reports 2019 9:1* [online]. 7 May 2019. Vol. 9, no. 1, p. 1–10. [Accessed 22 February 2025]. DOI 10.1038/s41598-019-43499-7. Available from: https://www.nature.com/articles/s41598-019-43499-7
20. PRATA, Andrew T., MINGARI, Leonardo, FOLCH, Arnau, MACEDONIO, Giovanni and COSTA, Antonio. FALL3D-8.0: A computational model for atmospheric transport and deposition of particles, aerosols and radionuclides - Part 2: Model validation. *Geoscientific Model Development*. 25 January 2021. Vol. 14, no. 1, p. 409–436. DOI 10.5194/gmd-14-409-2021.
21. WORLD HEALTH ORGANIZATION. PROTECTION OF THE HUMAN ENVIRONMENT. Guidelines for iodine prophylaxis following nuclear accidents. *World Health Organization,*. 1999. P. 1–45.

22. JUNAKOVA, Natalia, DVORSKY, Tomas, VACLAVIK, Vojtech, BALINTOVA, Magdalena, LISZOKOVÁ, Petra, ŠKRKAL, Jan, STALMACHOVÁ, Barbara, ZÁHOROVÁ, Věra and PILÁTOVÁ, Helena. Occurrence of 137Cs in Soil and Agricultural and Forest Products of the Contaminated Northeastern Part of the Czech Republic. *Engineering Proceedings 2023, Vol. 57, Page 11* [online]. 30 November 2023. Vol. 57, no. 1, p. 11. [Accessed 22 February 2025]. DOI 10.3390/ENGPROC2023057011. Available from: https://www.mdpi.com/2673-4591/57/1/11/htm
23. PUCKETT, Yana, AL-NASER, Yousif A. and NAPPE, Thomas M. Ionizing Radiation. *Encyclopedia of Genetics, Genomics, Proteomics and Informatics* [online]. 17 December 2023. P. 1625–1625. [Accessed 4 February 2025]. DOI 10.1007/978-1-4020-6754-9_14028. Available from: https://www.ncbi.nlm.nih.gov/sites/books/NBK534237/
24. KHALED, Saman and HELD, Kathryn D. Radiation Biology: A Handbook for Teachers and Students. *International Journal of Radiation Biology* [online]. 2012. Vol. 88, no. 11, p. 858–859. [Accessed 4 October 2023]. DOI 10.3109/09553002.2012.666006. Available from: https://www.iaea.org/publications/8219/radiation-biology-a-handbook-for-teachers-and-students
25. JIAO, Yunfei, CAO, Fangyu and LIU, Hu. *Radiation-induced Cell Death and Its Mechanisms* [online]. 1 November 2022. Lippincott Williams and Wilkins. [Accessed 4 February 2025]. Available from: https://pmc.ncbi.nlm.nih.gov/articles/PMC9512240/
26. THIERRY-CHEF, Isabelle, CARDIS, Elisabeth, DAMILAKIS, John, FRIJA, Guy, HIERATH, Monika and HOESCHEN, Christoph. *Medical applications of ionizing radiation and radiation protection for European patients, population and environment* [online]. 2022. EDP Sciences. [Accessed 4 February 2025]. Available from: https://www.epj-n.org/articles/epjn/full_html/2022/01/epjn220013/epjn220013.html
27. GIBBONS, John P. *Khan's the physics of radiation therapy (6th Edition)* [online]. 2019. [Accessed 11 May 2025]. ISBN 9781496397539. Available from: https://books.google.com/books?hl=en&lr=&id=cvtPBAAAQBAJ&oi=fnd&pg=PP1&dq=Khan%27s+The+Physics+of+Radiation+Therapy&ots=uyZawxslab&sig=3dxLYAG1sjICbmBFcBXbd6fH1j0
28. DENDY, P P and HEATON, B. *Physics for diagnostic radiology: Third edition*. 2011. ISBN 9781439896921.
29. VAÑÓ, E, MILLER, C.J., REHANI, M.M., KANG, K., ROSENSTEIN, M., ORTIZ-LÓPEZ, P., MATTSSON, S., PADOVANI, R. and ROGERS, A. *ICRP Publication 130* [online]. 2015. [Accessed 4 February 2025]. ISBN 9781473939509. Available from: http://ani.sagepub.com/
30. SAENKO, Vladimir and MITSUTAKE, Norisato. *Radiation-Related Thyroid Cancer* [online]. 4 January 2024. Oxford Academic. [Accessed 4 February 2025]. Available from: https://dx.doi.org/10.1210/endrev/bnad022
31. INTERNATIONAL AGENCY FOR RESEARCH ON CANCER. *A review of human carcinogens. Part D: Radiation.* International Agency for Research on Cancer, 2012.
32. MOTT, J. H.L. and DANIEL, J. M. *Interactions of Electromagnetic Radiation and Subatomic Particles with Matter – Part 1* [online]. 1 July 2021. Elsevier Ltd. [Accessed 6 February 2025]. Available from: http://www.clinicaloncologyonline.net/article/S0936655521000479/fulltext
33. ZHANG, Quanshi, WANG, Xiwen, SUN, Qiyin, JIN, Yuehui, LI, Yun, LI, Ziyu, SUN, Tao and WANG, Liang. Investigation and Application of High Megavoltage X-Ray Imaging Mode in Radiotherapy. *International Journal of Medical Physics, Clinical Engineering and Radiation Oncology*. 2016. Vol. 05, no. 01, p. 42–50. DOI 10.4236/ijmpcero.2016.51005.
34. PODGORSAK, E B. Slide set of 194 slides based on the chapter authored by E.B. Podgorsak of the IAEA publication (ISBN 92-0-107304-6): Review of Radiation Oncology Physics: A Handbook for Teachers and Students Chapter 1: Basic Radiation Physics. . 2006.
35. LOWDON, Matthew, MARTIN, Peter G., HUBBARD, M. W.J., TAGGART, M. P.,

CONNOR, Dean T., VERBELEN, Yannick, SELLIN, P. J. and SCOTT, Thomas B. Evaluation of Scintillator Detection Materials for Application within Airborne Environmental Radiation Monitoring. *Sensors (Basel, Switzerland)* [online]. 2 September 2019. Vol. 19, no. 18, p. 3828. [Accessed 5 March 2025]. DOI 10.3390/S19183828. Available from: https://pmc.ncbi.nlm.nih.gov/articles/PMC6767284/

36. LIN, Ziyu, LV, Shichao, YANG, Zhongmin, QIU, Jianrong and ZHOU, Shifeng. Structured Scintillators for Efficient Radiation Detection. *Advanced Science* [online]. 1 January 2021. Vol. 9, no. 2, p. 2102439. [Accessed 5 March 2025]. DOI 10.1002/ADVS.202102439. Available from: https://pmc.ncbi.nlm.nih.gov/articles/PMC8805559/
37. KERLIN, Thomas W. and UPADHYAYA, Belle R. Nuclear plant instrumentation. *Dynamics and Control of Nuclear Reactors*. 1 January 2019. P. 213–235. DOI 10.1016/B978-0-12-815261-4.00016-0.
38. ZHANG, Xi, XIE, Qiangqiang, XIE, Siwei, YU, Xin, XU, Jianfeng and PENG, Qiyu. A Novel Portable Gamma Radiation Sensor Based on a Monolithic Lutetium-Yttrium Oxyorthosilicate Ring. *Sensors (Basel, Switzerland)* [online]. 2 May 2021. Vol. 21, no. 10, p. 3376. [Accessed 5 March 2025]. DOI 10.3390/S21103376. Available from: https://pmc.ncbi.nlm.nih.gov/articles/PMC8150370/
39. CAPAN, Ivana. Wide-Bandgap Semiconductors for Radiation Detection: A Review. *Materials 2024, Vol. 17, Page 1147* [online]. 1 March 2024. Vol. 17, no. 5, p. 1147. [Accessed 8 March 2025]. DOI 10.3390/MA17051147. Available from: https://www.mdpi.com/1996-1944/17/5/1147/htm
40. GAMAGE, Kelum A A and TAYLOR, C James. *Radiation Sensing: Design and Deployment of Sensors and Detectors* [online]. 2021. [Accessed 8 March 2025]. Available from: www.mdpi.com/journal/sensors
41. HE, Rui, NIU, Xiao-Yang, WANG, Yi, LIANG, Hong-Wei, LIU, Hong-Bang and TIAN, Ye. Advances in nuclear detection and readout techniques. *Nuclear Science and Techniques* [online]. 2023. Vol. 34, p. 205. [Accessed 8 March 2025]. DOI 10.1007/s41365-023-01359-0. Available from: https://doi.org/10.1007/s41365-023-01359-0
42. OJO, A. A., CRANTON, W. M. and DHARMADASA, I. M. Introduction to Photovoltaics. *Next Generation Multilayer Graded Bandgap Solar Cells* [online]. 2019. P. 1–15. [Accessed 8 March 2025]. DOI 10.1007/978-3-319-96667-0_1. Available from: https://link.springer.com/chapter/10.1007/978-3-319-96667-0_1
43. ZHANG, Jianyong, MO, Xiaohu and CAI, Xiao. Study of Annealing the Damaged HPGe Detector *. *World Journal of Nuclear Science and Technology* [online]. 2021. Vol. 11, p. 100–108. [Accessed 8 March 2025]. DOI 10.4236/wjnst.2021.112007. Available from: https://doi.org/10.4236/wjnst.2021.112007
44. PRINCIPATO, Fabio, BETTELLI, Manuele, ZAPPETTINI, Andrea and ABBENE, Leonardo. A Novel Extraction Procedure of Contact Characteristic Parameters from Current-Voltage Curves in CdZnTe and CdTe Detectors. *Sensors (Basel, Switzerland)* [online]. 1 July 2023. Vol. 23, no. 13. [Accessed 8 March 2025]. DOI 10.3390/S23136075. Available from: https://pubmed.ncbi.nlm.nih.gov/37447923/
45. INABA, Yohei, NAKAMURA, Masaaki, ZUGUCHI, Masayuki and CHIDA, Koichi. Development of Novel Real-Time Radiation Systems Using 4-Channel Sensors. *Sensors 2020, Vol. 20, Page 2741* [online]. 11 May 2020. Vol. 20, no. 9, p. 2741. [Accessed 8 March 2025]. DOI 10.3390/S20092741. Available from: https://www.mdpi.com/1424-8220/20/9/2741/htm
46. KATO, Masahiro, ISHII, Junya, TANAKA, Hiroyuki, SUGIYAMA, Midori and KUROSAWA, Tadahiro. Portable Gamma Irradiation System with ^{57}Co, ^{133}Ba, ^{137}Cs, and ^{60}Co for On-site Calibration of Environmental Radiation Monitoring Devices. *Journal of Radiation Protection and Research* [online]. 23 December 2024. Vol. 49, no. 4, p. 166–173. [Accessed 10 March 2025]. DOI 10.14407/JRPR.2024.00066. Available from: http://www.jrpr.org/journal/view.php?number=1176

47. STROSCHEIN and THOMAS. Performing Radiation & Contamination Surveys RP02.02. . 2020.
48. TITUS, Deena, SAMUEL, E. James Jebaseelan and ROOPAN, Selvaraj Mohana. Radiation Dosimetry—A Different Perspective of Polymer Gel. In : [online]. Springer, Singapore, 2018. p. 309–341. [Accessed 19 July 2023]. ISBN 978-981-10-6086-1. Available from: https://link.springer.com/chapter/10.1007/978-981-10-6086-1_8
49. DAVIES, J. B. and BALDOCK, C. Sensitivity and stability of the Fricke-gelatin-xylenol orange gel dosimeter. *Radiation Physics and Chemistry*. 1 June 2008. Vol. 77, no. 6, p. 690–696. DOI 10.1016/j.radphyschem.2008.01.007.
50. EL GOHARY, M. I., SOLIMAN, Y. S., AMIN, E. A., GAWAD, M. H.Abdel and DESOUKY, O. S. Effect of perchloric acid on the performance of the Fricke xylenol gel dosimeter. *Applied Radiation and Isotopes*. 1 July 2016. Vol. 113, p. 66–69. DOI 10.1016/j.apradiso.2016.04.024.
51. SOLIMAN, Yasser S., BESHIR, W. B., ABDELGAWAD, Mahmoud H., BRÄUER-KRISCH, Elke and ABDEL-FATTAH, A. A. Pergascript orange-based polymeric solution as a dosimeter for radiotherapy dosimetric validation. *Physica Medica*. 1 January 2019. Vol. 57, p. 169–176. DOI 10.1016/j.ejmp.2019.01.005.
52. ABOELEZZ, Eslam and POGUE, Brian W. *Review of nanomaterial advances for ionizing radiation dosimetry* [online]. 1 June 2023. American Institute of Physics Inc. [Accessed 24 November 2023]. Available from: /aip/apr/article/10/2/021312/2893695/Review-of-nanomaterial-advances-for-ionizing
53. PATHAK, Ashima. Dosimetry and Safety Issues. *Tools and Techniques in Radiation Biophysics* [online]. 2023. P. 267–288. [Accessed 11 March 2025]. DOI 10.1007/978-981-99-6086-6_14. Available from: https://link.springer.com/chapter/10.1007/978-981-99-6086-6_14
54. EYADEH, Molham M., RABAEH, Khalid A., ALSHOMALI, Laith S., DIAMOND, Kevin R. and OGLAT, Ammar A. Evaluation of a novel physically cross-linked fricke-xylenol orange-polyvinyl alcohol radio-chromic gel dosimeter for radiotherapy. *Radiation Measurements*. 1 September 2024. Vol. 177, p. 107263. DOI 10.1016/j.radmeas.2024.107263.
55. ROUSSEAU, Alice, STIEN, Christel, BORDY, Jean Marc and BLIDEANU, Valentin. Fricke-Xylenol orange-Gelatin gel characterization with dual wavelength cone-beam optical CT scanner for applications in stereotactic and dynamic radiotherapy. *Physica Medica*. 1 May 2022. Vol. 97, p. 1–12. DOI 10.1016/j.ejmp.2022.03.008.
56. ABOELEZZ, E., SHARAF, M. A., HASSAN, G. M. and EL-KHODARY, A. Nano-barium-strontium sulfate as a new thermoluminescence dosimeter. *Journal of Luminescence*. 1 October 2015. Vol. 166, p. 156–161. DOI 10.1016/j.jlumin.2015.05.026.
57. CIOLACU, Elena, CIOLACU, Florin, ERDEM SAGSOZ, Mustafa, KORKUT, Ozlem and GALLO, Salvatore. Advancements in Tissue-Equivalent Gel Dosimeters. *Gels 2025, Vol. 11, Page 81* [online]. 21 January 2025. Vol. 11, no. 2, p. 81. [Accessed 6 February 2025]. DOI 10.3390/GELS11020081. Available from: https://www.mdpi.com/2310-2861/11/2/81/htm
58. 103, ICRP Publ. Recommendations of the international commission on radiological protection. *Health Physics* [online]. 1959. Vol. 2, no. 1, p. 1–20. [Accessed 12 November 2024]. DOI 10.1097/00004032-195901000-00001. Available from: https://cir.nii.ac.jp/crid/1573950401126566016
59. BOICE JR, JD, COOPER, Usa JR, LEE, Uk J, LOCHARD, Korea J, CLARKE, RH, METTLER JR, Fa, STEWART AKLEYEV M HAUER-JENSEN JH HENDRY NJ KLEIMAN TJ MACVITTIE, Fa AV and ALEMAN EDGAR K MABUCHI CR MUIRHEAD RE SHORE WH WALLACE, BM AB. Annals of the ICRP Published on behalf of the International Commission on Radiological Protection International Commission on Radiological Protection Members of the 2010-2013 Main Commission of the ICRP. . 2011.
60. FARTODE, Anoop P, FARTODE, Swati A and SHELKE, Tushar R. GAMMA RADIATION

INDUCED DECOLORIZATION OF INDIGO CARMINE DYE SOLUTIONS. . 2019. No. 6, p. 2394– 0697.

61. KANJAL, Muhammad Imran, MUNEER, Majid, JAMAL, Muhammad Asghar, BOKHARI, Tanveer Hussain, WAHID, Abdul, ULLAH, Shafqat, AMRANE, Abdeltif, HADADI, Amina, TAHRAOUI, Hichem and MOUNI, Lotfi. A Study of Treatment of Reactive Red 45 Dye by Advanced Oxidation Processes and Toxicity Evaluation Using Bioassays. *Sustainability (Switzerland)* [online]. 2023. Vol. 15, no. 9. [Accessed 4 September 2024]. DOI 10.3390/su15097256. Available from: https://hal.science/hal-04115493
62. ARSHAD, Rabia, BOKHARI, Tanveer H., KHOSA, Kaleem K., BHATTI, Ijaz A., MUNIR, Majid, IQBAL, Mazhar, IQBAL, Dure N., KHAN, M. I., IQBAL, Munawar and NAZIR, Arif. Gamma radiation induced degradation of anthraquinone Reactive Blue-19 dye using hydrogen peroxide as oxidizing agent. *Radiation Physics and Chemistry*. 1 March 2020. Vol. 168, p. 108637. DOI 10.1016/j.radphyschem.2019.108637.
63. CLAYDEN, Jonathan, GREEVES, Nick and WARREN, Stuart. *Organic Chemistry Organic Chemistry—online support* [online]. 2001. [Accessed 4 September 2024]. Available from: www.oxfordtextbooks.co.uk/orc/clayden2e/
64. ANDŔS, C., DEL CASTILLO, A., TORTOSA, R., ALONSO, D. and BARQUERO, R. A comprehensive study of the Gafchromic EBT2 radiochromic film. A comparison with EBT. *Medical Physics*. 2010. Vol. 37, no. 12, p. 6271–6278. DOI 10.1118/1.3512792.
65. ALQATHAMI, Mamdooh, BLENCOWE, Anton, QIAO, Greg, BUTLER, Duncan and GESO, Moshi. Optimization of the sensitivity and stability of the PRESAGE™ dosimeter using trihalomethane radical initiators. *Radiation Physics and Chemistry*. July 2012. Vol. 81, no. 7, p. 867–873. DOI 10.1016/J.RADPHYSCHEM.2012.03.022.
66. CHO, Jin Dong, SON, Jaeman, CHOI, Chang Heon, KIM, Jin Sung, WU, Hong Gyun, PARK, Jong Min and KIM, Jung in. Improvement in sensitivity of radiochromic 3D dosimeter based on rigid polyurethane resin by incorporating tartrazine. *PLoS ONE* [online]. 2020. Vol. 15, no. 3, p. e0230410. [Accessed 11 February 2025]. DOI 10.1371/journal.pone.0230410. Available from: https://pmc.ncbi.nlm.nih.gov/articles/PMC7075553/
67. ALASHRAH, Saleh, EL-GHOUL, Yassine and OMER, Mohammed Ahmed Ali. Synthesis and characterization of a new nanocomposite film based on polyvinyl alcohol polymer and nitro blue tetrazolium dye as a low radiation dosimeter in medical diagnostics application. *Polymers* [online]. 1 June 2021. Vol. 13, no. 11. [Accessed 11 December 2023]. DOI 10.3390/polym13111815. Available from: https://pubmed.ncbi.nlm.nih.gov/34072823/
68. KOBAYASHI, K., USAMI, N., PORCEL, E., LACOMBE, S. and LE SECH, C. *Enhancement of radiation effect by heavy elements* [online]. April 2010. Mutat Res. [Accessed 27 November 2023]. Available from: https://pubmed.ncbi.nlm.nih.gov/20074660/
69. SUTANTO, Heri, LO, Nixon Kenny, ALKIAN, Ilham, TRIADYAKSA, Pandji, MARHAENDRAJAYA, Indras, JONATHAN, Felix, IRVIANDI, Risnu and ARIFIN, Zaenal. Developing a novel radiosensitive metal ion-loaded PVA/NBT film as medical low-dose X-ray dosimeter. *Radiation Physics and Chemistry*. 1 November 2024. Vol. 224, p. 112078. DOI 10.1016/j.radphyschem.2024.112078.
70. ALBEJADI, Reham, ULLAH, Zabih, EL-TAHER, Atef and ALASHRAH, Saleh. Selection of the Optimal Concentration of Nitro Blue Tetrazolium Dye in Polyvinyl Alcohol Film for Diagnostic Radiology. *Trends in Sciences* [online]. 1 October 2024. Vol. 21, no. 11, p. 8037. [Accessed 11 February 2025]. DOI 10.48048/tis.2024.8037. Available from: https://tis.wu.ac.th/index.php/tis/article/view/8037
71. JASZCZAK, Malwina, SĄSIADEK-ANDRZEJCZAK, Elżbieta and KOZICKI, Marek. Discolouring 3D Gel Dosimeter for UV Dose Distribution Measurements. *Materials* [online]. 30 March 2022. Vol. 15, no. 7, p. 2546. [Accessed 15 November 2024]. DOI 10.3390/ma15072546. Available from: https://www.mdpi.com/1996-1944/15/7/2546/htm

72. LOUSADA, Cláudio M., SOROKA, Inna L., YAGODZINSKYY, Yuriy, TARAKINA, Nadezda V., TODOSHCHENKO, Olga, HÄNNINEN, Hannu, KORZHAVYI, Pavel A. and JONSSON, Mats. Gamma radiation induces hydrogen absorption by copper in water. *Scientific Reports*. 18 April 2016. Vol. 6. DOI 10.1038/srep24234.

73. KOLB, Doris. Oxidation states of manganese. *Journal Of Chemical Education* [online]. 1988. Vol. 65, no. 11, p. 1004–1005. [Accessed 12 August 2024]. DOI 10.1021/ED065P1004.2. Available from: https://pubs.acs.org/doi/pdf/10.1021/ed065p1004.2

74. GHALEI, Mohammad, VANDENBORRE, Johan, BLAIN, Guillaume, HADDAD, Ferid, MOSTAFAVI, Mehran and FATTAHI, Massoud. Oxidation and/or reduction of manganese species by γ-ray and He2+ particle irradiation in highly concentrated carbonate media. *Radiation Physics and Chemistry*. 1 February 2016. Vol. 119, p. 142–150. DOI 10.1016/j.radphyschem.2015.10.009.

75. PUSPALATA, R., SUMATHI, S., CHANDRAMOHAN, P., BERA, S., RANGARAJAN, S., SUDHA, R., NARASIMHAN, S. V. and VELMURUGAN, S. Gamma radiation induced formation and characterization of the nano-oxides of manganese. *Radiation Physics and Chemistry*. 1 April 2013. Vol. 85, p. 152–160. DOI 10.1016/j.radphyschem.2012.12.018.

76. SILBERBERG, Martin. The d-Block Elements. In : *Principles of General Chemistry (v. 1.0)* [online]. 2009. p. 493–532. [Accessed 22 November 2024]. Available from: https://2012books.lardbucket.org/books/principles-of-general-chemistry-v1.0/s27-the-d-block-elements.html

77. MIYOSHI, Hirokazu, MASHIKO, Yuji, MAEDA, Sunao, YAMADA, Kenji and MASTUMURA, Jiro. Reversible radiochromic plate based on polyvinyl alcohol-iodide complex containing silica nanoparticles. *Journal of Radioanalytical and Nuclear Chemistry* [online]. 1 May 2016. Vol. 308, no. 2, p. 469–475. [Accessed 21 August 2024]. DOI 10.1007/s10967-015-4465-y. Available from: https://link.springer.com/article/10.1007/s10967-015-4465-y

78. WELTI, Sophia E., MIYOSHI, Hirokazu and YASUDA, Hiroshi. Radiochromic reactions in repetitive X-ray irradiations of a novel gel complex composed of polyvinyl alcohol, iodide, and silica nanoparticles (PAISiN). *Radiation Measurements*. 1 July 2024. Vol. 175, p. 107173. DOI 10.1016/j.radmeas.2024.107173.

79. GALIGA, Henley F. and SEVILLA, Fortunato B. Microscale assessment of iodate fortificant in food-grade salt using the potassium iodide/polyvinyl alcohol colorimetric reagent. *Journal of Food Composition and Analysis*. 1 July 2022. Vol. 110, p. 104558. DOI 10.1016/j.jfca.2022.104558.

80. HAYASHI, Shin Ichiro, ONO, Kaoru, FUJINO, Keisuke and KURIHARA, Ryosuke. Effects of PVA-GTA-I radiochromic gel dosimeter components on optical dose-response. In : *Journal of Physics: Conference Series* [online]. IOP Publishing, 1 January 2022. p. 012014. [Accessed 26 August 2024]. Available from: https://iopscience.iop.org/article/10.1088/1742-6596/2167/1/012014

81. TAÑO, Jolan E., GONZALES, Chryzel Angelica B., SAITO, Akito, WADA, Takuya, NAGATA, Yasushi and YASUDA, Hiroshi. Annealing properties of the PVA-GTA-I gel dosimeter. *Radiation Measurements*. 1 December 2021. Vol. 149, p. 106674. DOI 10.1016/j.radmeas.2021.106674.

82. RABAEH, Khalid A., AL-ZAWAYDAIH, Hashem H.N., EYADEH, Molham M. and SHATNAWI, Moneeb T.M. High optical stability of reusable radiochromic polyvinyl alcohol-iodine gel dosimeter for radiotherapy. *Radiation Physics and Chemistry*. 1 October 2022. Vol. 199, p. 110338. DOI 10.1016/j.radphyschem.2022.110338.

83. RABAEH, Khalid A, QAWOUQ, Ruba K.A., EYADEH, Molham M and SHATNAWI, Moneeb T.M. Optimizing the feasibility of polyvinyl alcohol-potassium iodine gel for medical dosimeter. *Biomedical Physics and Engineering Express* [online]. 10 July 2024. Vol. 10, no. 5, p. 055006. [Accessed 2 September 2024]. DOI 10.1088/2057-1976/ad5db0. Available from:

https://iopscience.iop.org/article/10.1088/2057-1976/ad5db0

84. MAKHAYEVA, D. N., IRMUKHAMETOVA, G. S. and KHUTORYANSKIY, V. V. Polymeric Iodophors: Preparation, Properties, and Biomedical Applications. *Review Journal of Chemistry* [online]. January 2020. Vol. 10, no. 1, p. 40. [Accessed 22 March 2025]. DOI 10.1134/S2079978020010033. Available from: https://pmc.ncbi.nlm.nih.gov/articles/PMC7749746/

85. AWTREY, Alice D. and CONNICK, Robert E. The Absorption Spectra of I2, I3−, I−, IO3−, S4O6− and S2O3−. Heat of the Reaction I3− = I2 + I−. *Journal of the American Chemical Society*. 1 April 1951. Vol. 73, no. 4, p. 1842–1843. DOI 10.1021/ja01148a504.

86. VO, Mokhnach. Iodine and the Problems of Life: The Theory of the Biological Activity of Iodine and the Problems of the Practical Use of Iodine Compounds with High Polymers. *Nauka* [online]. 1974. [Accessed 22 March 2025]. Available from: https://scholar.google.com/scholar?hl=en&as_sdt=0%2C5&as_ylo=1974&as_yhi=1974&q=Iod+i+problemy+zhizni+%28Teoriya+biologicheskoj+aktivnosti+ioda+i+problemy+prakticheskogo+primeneniya+soedinenij+ioda+s+vysokopolimerami%29&btnG=

87. NOGUCHI, H, … H Jyodai - Journal of Polymer Science and 1997, undefined. Formation of poly (vinyl alcohol)–iodine complexes in solution. *Wiley Online LibraryH Noguchi, H Jyodai, S MatsuzawaJournal of Polymer Science Part B: Polymer Physics, 1997•Wiley Online Library* [online]. [Accessed 22 March 2025]. Available from: https://onlinelibrary.wiley.com/doi/abs/10.1002/(SICI)1099-0488(199708)35:11%3C1701::AID-POLB4%3E3.0.CO;2-V

88. RAHN, Ronald O., GERSTENBERG, Henry M. and VAVRINA, Gerard A. Dosimetry of ionizing radiation using an iodide/iodate aqueous solution. *Applied Radiation and Isotopes*. 1 March 2002. Vol. 56, no. 3, p. 525–534. DOI 10.1016/S0969-8043(01)00143-9.

89. HAYASHI, Shin ichiro, ONO, Kaoru, FUJINO, Keisuke, IKEDA, Sachie and TANAKA, Kenichi. Novel radiochromic gel dosimeter based on a polyvinyl alcohol – Iodide complex. *Radiation Measurements*. 1 February 2020. Vol. 131, p. 106226. DOI 10.1016/j.radmeas.2019.106226.

90. FERNANDO, Ashantha, PARAJULI, Suman, BARAKOTI, Krishna K., MIAO, Wujian and ALPUCHE-AVILES, Mario A. Evidence of radical intermediate generated in the electrochemical oxidation of iodide. *Journal of the Mexican Chemical Society* [online]. 17 October 2019. Vol. 63, no. 3 Special Issue, p. 70–83. [Accessed 11 May 2025]. DOI 10.29356/jmcs.v63i3.529. Available from: http://www.scielo.org.mx/scielo.php?script=sci_arttext&pid=S1870-249X2019000300070&lng=es&nrm=iso&tlng=en

91. SONG, Yingxu, ZHANG, Sumei, KANG, Jian, CHEN, Jinyao and CAO, Ya. Water absorption dependence of the formation of poly(vinyl alcohol)-iodine complexes for poly(vinyl alcohol) films. *RSC Advances* [online]. 26 August 2021. Vol. 11, no. 46, p. 28785–28796. [Accessed 24 October 2024]. DOI 10.1039/d1ra04867h. Available from: https://pubs.rsc.org/en/content/articlehtml/2021/ra/d1ra04867h

92. ROYAL SOCIETY OF CHEMISTRY. *PVA polymer slime | Experiment | RSC Education* [online]. [Accessed 24 October 2024]. Available from: https://edu.rsc.org/experiments/pva-polymer-slime/756.article

93. KEIZO, Miyasaka. PVA-iodine complexes: Formation, structure, and properties. *Advances in Polymer Science* [online]. 1993. Vol. 108, p. 90–129. [Accessed 24 October 2024]. DOI 10.1007/3-540-56579-5_3. Available from: https://link.springer.com/chapter/10.1007/3-540-56579-5_3

94. KUDREVICIUS, Linas, JASELSKĖ, Evelina, STANKUS, Gabrielius, ARSLONOVA, Shirin and ADLIENE, Diana. Post-Irradiation Behavior of Colored PVA-Based Films Containing Ag Nanoparticles as Radiation Detectors/Exposure Indicators. *Gels* [online]. 24 April 2024. Vol. 10, no. 5, p. 290. [Accessed 12 December 2024]. DOI 10.3390/gels10050290. Available

from: https://www.mdpi.com/2310-2861/10/5/290/htm

95. SKOOG, D. A., HOLLER, F. J. and CROUCH, S. R. Principles of Instrumental Analysis 7th edition. [online]. 2018. [Accessed 3 May 2025]. DOI 10.1515/pac-2015-0305. Available from: http://www.chem.qmul.ac.uk/iupac/AtWt/
96. HARRIS, Daniel C. Quantitative Chemical Analysis (10th edition). *W.H. Freeman and Company*. [online]. 2020. [Accessed 3 May 2025]. Available from: https://scholar.google.com/scholar?hl=en&as_sdt=0%2C5&q=Harris%2C+D.+C.+%282020%29.+Quantitative+Chemical+Analysis+%2810th+ed.%29.+W.H.+Freeman.+—+Section+on+absorbance+and+transmittance+relationships&btnG=
97. BOLGAR, Peter. and ATKINS, P. W.. *Student solutions manual to accompany Atkins' Physical chemistry 11th edition*. Oxford University Press, 2018. ISBN 9780192550866.
98. OCEAN OPTICS. *Halogen Light Source Installation and Operation Manual*. 2009.
99. BARAKAT, M. F., EL-SALAMAWY, K., EL-BANNA, M., ABDEL-HAMID, M. and ABDEL-REHIM TAHA, A. Radiation effects on some dyes in non-aqueous solvents and in some polymeric films. *Radiation Physics and Chemistry* [online]. 2001. Vol. 61, no. 2, p. 129–136. [Accessed 17 November 2024]. DOI 10.1016/S0969-806X(01)00181-5. Available from: https://www.researchgate.net/publication/243348686_Radiation_effects_on_some_dyes_in_non-aqueous_solvents_and_in_some_polymeric_films
100. Potassium Iodate SDS. [online]. 2024. [Accessed 12 April 2025]. Available from: https://www.sigmaaldrich.com/LT/en/sds/aldrich/438464?userType=undefined
101. Sodium tetraborate SDS. [online]. 2024. [Accessed 12 April 2025]. Available from: https://www.sigmaaldrich.com/LT/en/sds/sial/b3545?userType=undefined
102. Potassium iodide SDS. [online]. 2024. [Accessed 12 April 2025]. Available from: https://www.sigmaaldrich.com/LT/en/sds/sigma/60399?userType=undefined
103. PANDEY, Shipra, PANDEY, Shiv K., PARASHAR, Vyom, MEHROTRA, G. K. and PANDEY, Avinash C. Ag/PVA nanocomposites: Optical and thermal dimensions. *Journal of Materials Chemistry* [online]. 21 November 2011. Vol. 21, no. 43, p. 17154–17159. [Accessed 22 December 2024]. DOI 10.1039/c1jm13276h. Available from: https://www.researchgate.net/publication/216446237_AgPVA_nanocomposites_Optical_and_thermal_dimensions
104. KIREEV, S. V. and SHNYREV, S. L. Study of molecular iodine, iodate ions, iodide ions, and triiodide ions solutions absorption in the UV and visible light spectral bands. *Laser Physics* [online]. 1 July 2015. Vol. 25, no. 7, p. 075602. [Accessed 22 December 2024]. DOI 10.1088/1054-660X/25/7/075602. Available from: https://ui.adsabs.harvard.edu/abs/2015LaPhy..25g5602K/abstract
105. MOHAMMED, M I, ISMAIL, A M and SALEM, G F. Structural, Optical and Thermal Properties of PVA / KI Based Solid Polymer Electrolyte. *Egyptian Journal of Solids* [online]. 1 November 2017. Vol. 40, no. 1, p. 79–94. [Accessed 23 December 2024]. DOI 10.21608/ejs.2017.148265. Available from: https://ejs.journals.ekb.eg/article_148265.html
106. TAÑO, J., HAYASHI, S., HIROTA, S., GONZALES, C. A. and YASUDA, H. Development of a reusable PVA-GTA-I gel dosimeter for 3D radiation dose assessments. In : *Journal of Physics: Conference Series*. Institute of Physics Publishing, 29 August 2019.
107. SULISTYARTI, Hermin, ATIKAH, Atikah, FARDIYAH, Qonitah, FEBRIYANTI, Sita and ASDAUNA, Asdauna. A Simple and Safe Spectrophotometric Method for Iodide Determination. *Makara Journal of Science* [online]. 31 July 2015. Vol. 19, no. 2. [Accessed 7 May 2025]. DOI 10.7454/mss.v19i2.4736. Available from: https://www.researchgate.net/publication/294721237_A_Simple_and_Safe_Spectrophotometric_Method_for_Iodide_Determination